ERJ Express. Published on July 5, 2018 as doi: 10.1183/13993003.01857-2017

EUROPEAN RESPIRATORY *journal*

FLAGSHIP SCIENTIFIC JOURNAL OF ERS

Early View

Original article

Macitentan reduces progression of TGF-β1-induced pulmonary fibrosis and pulmonary hypertension

Pierre-Simon Bellaye, Toyoshi Yanagihara, Elise Granton, Seidai Sato, Chiko Shimbori, Chandak Upagupta, Jewel Imani, Nathan Hambly, Kjetil Ask, Jack Gauldie, Marc Iglarz, Martin Kolb

Please cite this article as: Bellaye P-S, Yanagihara T, Granton E, *et al*. Macitentan reduces progression of TGF-β1-induced pulmonary fibrosis and pulmonary hypertension. *Eur Respir J* 2018; in press (https://doi.org/10.1183/13993003.01857-2017).

Macitentan reduces progression of TGF-β1-induced pulmonary fibrosis and pulmonary hypertension.

Pierre-Simon Bellaye[1,2*], Toyoshi Yanagihara[1*], Elise Granton[1], Seidai Sato[1,3], Chiko Shimbori[1], Chandak Upagupta[1], Jewel Imani[1], Nathan Hambly[1], Kjetil Ask[1], Jack Gauldie[1], Marc Iglarz[4], Martin Kolb[1]

[1]Firestone Institute for Respiratory Health, Research Institute at St Joseph's Healthcare, Dept of Medicine, McMaster University, Hamilton, ON, Canada.

[2]Centre George-François Leclerc (CGFL), plateforme d'imagerie et radiothérapie préclinique, Dijon, France,

[3]Dept of Respiratory Medicine and Rheumatology, Graduate School of Biomedical Sciences, Tokushima University, Tokushima, Japan.

[4]Actelion Pharmaceuticals Ltd. - Allschwil, Switzerland

* These authors contributed equally to this work

Macitentan reduces progression of TGF-β1 induced pulmonary fibrosis and pulmonary hypertension while pirfenidone only slows fibrosis progression.

Idiopathic pulmonary fibrosis (IPF) is a progressive disease with unknown cause. Two drugs, nintedanib and pirfenidone, have been shown to slow, but not stop disease progression. Pulmonary hypertension (PH) is a frequent complication in IPF patients associated with poor prognosis. Macitentan is a dual endothelin receptor antagonist which is approved for PAH treatment. We hypothesised that the treatment of AdTGF-β1-induced pulmonary fibrosis animals with macitentan will result in improvement of PH due to chronic lung disease and limitation of fibrosis progression.

Rats (Sprague Dawley) which received AdTGF-β1 were treated by daily gavage of macitentan (100 mg/kg/d), pirfenidone (0.5% food admix) or their combination from D14 to D28. At sacrifice, pulmonary artery pressure (PAP) was measured and fibrosis was evaluated by morphometric measurements and hydroxyproline.

AdTGF-β1 induced pulmonary fibrosis associated with significant pulmonary hypertension. Macitentan reduced the increase in PAP and both macitentan and pirfenidone stopped fibrosis progression from D14 to D28. Macitentan protected endothelial cells from myofibroblast differentiation and apoptosis while pirfenidone only protected fibroblasts-to-myofibroblast differentiation. Both drugs induced apoptosis of differentiated myofibroblasts *in vitro* and *in vivo*.

Our results demonstrate that dual endothelin receptor antagonism was effective on both PH and lung fibrosis while pirfenidone only affected fibrosis.

Idiopathic pulmonary fibrosis (IPF) is characterized by progressive lung tissue scarring and destruction of alveaolar architecture. The prevalence of IPF is 20-42/100,000 in the general population and up to 245/100,000 in the age group above 70 years. The prognosis of IPF is poor, with a mortality rate comparable to aggressive cancers. The precise cause of IPF remains elusive and treatment options are limited with only two approved drugs, nintedanib and pirfenidone, that have been shown to slow progression, but not stop the disease [1-3]. The pathogenesis of IPF is viewed as aberrant and uncontrolled alveolar repair in which differentiation and persistance of myofibroblasts represents a crucial event. Myofibroblasts clustered in fibroblastic foci are responsible of the abnormal accumulation of extracellular matrix (ECM). Transforming growth factor-β1 (TGF-β1) plays a key role in IPF by inducing myofibroblast differentiation [4].

PH is a recognized complication of IPF and a poor prognostic marker [5]. PH is characterized by a persistent increase in mean pulmonary arterial pressure (mPAP), greater than 25 mmHg [6]. Histologically, PH presents with endothelial cell (EC) injury and vascular smooth muscle cell (VSMC) proliferation. Endothelin-1 (ET-1) is a potent vasoconstrictor that binds to ETA and ETB receptors which are present on pulmonary fibroblasts, VSMC and EC [7]. ET-1 is expressed in IPF lungs and in bleomycin-induced pulmonary fibrosis [8]. Moreover, ET-1 favours myofibroblast differentiation, persistence and resistance to apoptosis [9]. Our group demonstrated that the adenovector-mediated gene transfer of active TGF-β1 (AdTGF-β1) in rodent lungs leads to progressive and severe fibrosis coupled with PH through decreased expression of vascular endothelial growth factor (VEGF), enhanced EC apoptosis, subsequent vascular rarefaction and TGF-β-driven media thickening [10]. Macitentan, is a dual ETA/ETB receptor antagonist approved for the treatment of PAH [6]. In the bleomycin rat model of lung fibrosis macitentan demonstrated efficacy in reducing right ventricle hypertrophy and pulmonary remodeling [11]. Despite promising preclinical data, the Macitentan USe in IPF Clinical (MUSIC) trialfailed to show benefits of the drug for IPF patients [12]. However, this trial was conducted in patients with mild to moderate IPF who probably did not (yet) have significant remodelling of the pulmonary vasculature and PH. Therefore, further studies are needed to understand the real impact of ET-1 blockers on advanced IPF.

We investigated the efficacy and mechanisms by which dual ET receptor antagonism affects lung fibrosis and PH induced by AdTGF-β1 in rats in comparison to pirfenidone. We demonstrate for the first time that macitentan, in addition to a regression of TGF-β1-induced PH, inhibited TGF-β1-induced lung fibrosis progression in rats.

Materials and Methods

See online supplementary material for detailed methods

Human samples

Plasma and tissue was collected with patients' consent and approval by the Hamilton Integrated Research Ethics Board (HIREB #00-1839). Control lung tissue was from patients undergoing surgery for cancer. Lung fibrosis tissue was from patients undergoing biopsy for unclear interstitial lung disease. The biopsies analysed in this study revealed a usual interstitial pneumonia (UIP) pattern.

Antibodies and reagents

Antibodies are α-smooth muscle actin (α-SMA) (ab7817, Abcam), pSmad3 (ab51451, Abcam), Smad3 (ab40854, Abcam), VEGF (ab1316, Abcam), Cleaved caspase-3 (#9661, cell signaling), ET-1 (ab117757, Abcam), CD31 (sc-1506, Santacruz biotech.), ETRA (ab117521, Abcam), ETRB (ab117529, Abcam), GAPDH (#5174, Cell signaling technology). Anti-rabbit HRP linked IgG (#7074, Cell Signaling Technology), Anti-mouse IgG HRP-linked Antibody (#7076, Cell Signaling Technology). For fluorescence microscopy, we used goat or donkey secondary antibody conjugated with Alexa Fluor-488 and Alexa Fluor-555 (Abcam). Human rET-1 (100-21, PerproTech) and human rTGF-β1 (240-B, R&D systems).

Cell culture

Human derived normal primary pulmonary artery smooth muscle cells (ATCC, PCS-100-023) and primary pulmonary artery endothelial cells (ATCC, PCS-100-022) were grown according to manufacturer's recommendations. Fibroblasts were obtained from humans during surgical biopsy (control and IPF) and grown in RPMI medium (ATCC, 30-2001) supplemented with 10% FBS. All cells were incubated at 37°C, 5% CO_2.

Animal Experiments

Animal work was conducted under the guidelines from the Canadian Council on Animal Care and approved by the Animal Research Ethics Board of McMaster University (#13-12-48). Pulmonary fibrosis was induced by adenoviral vector encoding biologically active TGF-β1 (AdTGF-β1). Female Sprague-Dawley rats (225–250 g; Charles River, Wilmington, MA) received 5.0 x 10^8 PFU of AdTGF-β1 by intratracheal instillation under isoflurane anesthesia at D0. Rats received either macitentan (daily gavage 100 mg/kg/d, Actelion pharmaceuticals Ltd., Switzerland), pirfenidone (0.5% food admix, ad libitum, Chemcia Scientific, USA) or a

combination of both (n=6 per group) from D14 to 28. Before sacrifice, rats were anesthetised and a catheter (PE tubing, SP0109, ADInstruments Inc, USA) was introduced in the jugular vein and pushed further into the pulmonary artery to read the PAP with a pressure transducer (MLT844, ADInstruments Inc, USA). Afterwards, lungs were harvested and fixed in 10% formalin for histology or flash frozen in liquid nitrogen for protein and RNA analysis.

CT scan imaging

See online supplement for details

Western blotting

See online supplement for details

Hydroxyproline assay

Hydroxyproline content in lung tissue was measured by a colorimetric assay as described previously [13]. See online supplement for details

Ashcroft score

Pulmonary fibrosis of Masson Trichrome stained lung sections was graded from 0 (normal) to 8 (completely fibrotic lung), using a modified Ashcroft score [14].

Isolation of mRNA and gene expression

Total RNA was extracted from frozen lung tissue with TRIzol® reagent (Thermo fisher scientific, 15596026). Two µg of total RNA was reverse transcribed using qScript cDNA Super Mix (Quanta Bioscience, 95048-025, Gaithersburg, MD). The cDNA was amplified using a Fast 7500 real-time PCR system (AB Applied Biosystems) using TaqMan® Universal PCR Master Mix and predesigned primer pairs (Life Technologies, 4304437, Burlington, ON, Canada) for Collagen1A (Hs00164004_m1), TGFβR1 (Hs00610320_m1), ACTA2 (Hs00426835_g1) and 18S (Hs03003631_g1).

Histology and immunohistochemistry

Lung slides were stained with Masson Trichrome (MT) or Picrosirius Red (PSR). Picture acquisition were performed using an Automatic slide scanner microscope (Olympus VS 120-L). Endothelial Diameter (ED) was defined as distance between external elastic laminae, while Medial Wall Thickness (MWT) was determined as distance between external and

internal elastic laminae. Vessels were categorized as follows: Small: ED < 50 μm and large: ED > 50 μm. MWT was calculated using the following formula: MWT (%) = (2 × MT/ED) × 100%.

Immunofluorescence

See online supplement for details

ELISA

The levels of active TGF-β1, VEGF and ET-1 in rat and human BALF supernatants and sera were measured using a rat TGF-β1-specific ELISA kit (MB100B, R&D Systems), a rat VEGF ELISA kit (abcam, ab100786), a rat ET-1 ELISA kit (E-EL-R0167, Elabscience) and a human ET-1 ELISA kit (R&D Systems, DET100) respectively, according to the manufacturer's recommendations.

Contraction assay

See online supplement for details

Statistical Analysis

All data were expressed as mediane with interquartile range. Statistical analysis between two groups was performed using a non-parametric Mann-Whitney test. Statistical analysis between multiple groups with one control group was performed by Kruskal-Wallis test, with Dunn comparison test (post hoc). Analysis was performed with GraphPad Prism 6.0 (GraphPad Software Inc.). A p-value less than 0.05 was considered significant.

Results

The ET-1 system is activated in IPF patients

Circulating ET-1 was measured in sera of 31 IPF patients and 9 aged-matched healthy controls. ET-1 was significantly upregulated in IPF (Fig. 1A). Circulating ET-1 correlated with predicted Forced Vital Capacity (FVC) and Total Lung Capacity (TLC; Fig. 1B). Upregulation of the expression of the ET receptor ETRA was shown compared to control. Interestingly, the expression of ERTA was higher in advanced compared to moderate IPF (Fig. 1C). No difference between groups was found for the expression of the other ET receptor, ETRB (Fig. 1D).

Macitentan is preventing PH induced by TGF-β1 in rats

Mean pulmonary artery pressure (mPAP) significantly increased from D14 to D28 in AdTGF-β1 rats compared to controls (Fig2A). At D28, animals that received pirfenidone from D14 to D28 showed a non-significant decrease in mPAP while macitentan normalized the increase in mPAP induced by AdTGF-β1 (Fig. 2A). Animals that received the combination of macitentan and pirfenidone presented a similar mPAP reduction than animals receiving macitentan alone (Fig. 2A).

The increase in mPAP in AdTGF-β1 rats correlated with an increase in ET-1 in BALF but not in sera from D14 up to D28 compared to control (Fig.2B). While pirfenidone had no effect on ET-1, macitentan significantly reduced ET-1 in BALF when administered alone or in combination (Fig. 2B).

CT imaging allowed the quantification of vascular volume and density on large vessels (>75 μm) and demonstrated that AdTGF-β1 induced a decrease in lung vascular density and vascular volume which was inhibited by macitentan alone or in combination; pirfenidone had no effect (Fig. 2C-D). In addition, the number of small and large pulmonary vessels (ED: small: ED< 50 μm; large: ED > 50 μm) at D28 in AdTGF-β1 animals was significantly reduced (Supplemental figure 1A). Macitentan, but not pirfenidone, restored the number of both small and large vessels to levels comparable with controls. Vascular remodelling, assessed by medial wall thickness (MWT), was increased by D28 after AdTGF-β1 for small and large vessels (Supplemental figure 1B-C). This increase in MWT was significantly reduced by macitentan and combination treatment (Supplemental figure 1B-C).

Macitentan is modulating VEGF expression in AdTGF-β1 treated rats

AdTGF-β1 induced an increase in VEGF in BALF but not serum at D28 (Fig. 3A). Interestingly, macitentan significantly inhibited the VEGF increase induced by AdTGF-β1 in BALF and induced an increase in serum VEGF (Fig. 3A). Pirfenidone had no effect on VEGF (Fig. 3A). The effect of TGF-β1 on VEGF increase was confirmed in lung tissue from AdTGF-β1 rats at D28 (Fig. 3B); macitentan and combination therapy decreased VEGF expression, pirfenidone had no effect (Fig. 3B). AdTGF-β1 induced a dramatic upregulation of VEGF expression in the parenchyma at D28 while no VEGF positive EC were found (Fig. 3C and Supplemental figure 2A). On the contrary, macitentan alone or in combination reduced the expression of VEGF while increasing VEGF in EC (Fig. 3C and Supplemental figure 2A). Pirfenidone caused a similar expression of VEGF as AdTGF-β1 (Fig. 3C and

Supplemental figure 2A). These results have been confirmed on lung tissue by co-staining of CD31 and VEGF by immunofluorescence (Supplemental figure 3A-B).

Macitentan and pirfenidone prevent the progression of AdTGF-β1 induced lung fibrosis

Hydroxyproline levels in AdTGF-β1 rats were increased compared to control AdDL from D14 up to D28 (Fig. 4A). Macitentan, pirfenidone and their combination significantly lowered hydroxyproline content at D28 (Fig. 4A). AdTGF-β1 animals showed higher Ashcroft scores (Fig 4B) compared to control. Ashcroft scores from animals receiving macitentan, pirfenidone and combination therapy were reduced compared to AdTGF-β1 (Fig 4B). AdTGF-β1 rats presented an increase in fibrotic-area/whole-area ratio from D14 to D28 compared to control (quantitative assessment using ImageJ; Fig. 4B-C). Macitentan, pirfenidone and combination reduced the percentage of fibrotic area compared to AdTGF-β1 (Fig. 4B-C). PSR staining was increased by AdTGF-β1 and was prevented by macitentan, pirfenidone and the combination therapy at D28 (Fig. 4D). Interestingly, pressure-volume loops measurments at D28 demonstrated that both pirfenidone and macitentan induced an improvement in lung function compared with AdTGF-β1 treated rats (Supplemental figure 4A). In addition, CT scan allowed the quantification of area of fibrosis in 3D reconstructed lungs and demonstrated that macitentan and pirfenidone reduced significantly lung fibrosis induced by TGF-β1 (Supplemental figure 4B).

Macitentan and pirfenidone inhibit pro-fibrotic pathways in vivo in AdTGF-β1 rats

At D28 endogenous total and active TGF-β1 was upregulated compared to controls (Fig. 5A). Treatment with macitentan, pirfenidone and the combination inhibited TGF-β1 upregulation. AdTGF-β1 induced upregulation of TGF-β1 at D28 correlated with an increase in α-SMA (Fig. 4B). Smad3 phosphorylation, the main pathway of TGF-β1, was upregulated in AdTGF-β1 animals at D28. Interestingly, macitentan and, to a lesser extent, pirfenidone reduced AdTGF-β1-induced α-SMA and p-Smad3 upregulation (Fig. 5B). The combination of macitentan and pirfenidone had a comparable effect to macitentan alone (Fig. 5B). While AdTGF-β1 had no effect on ETRB, it significantly upregulated ETRA and ET-1 expression. Again, macitentan, pirfenidone and their combination inhibited both ETRA and ET-1 upregulation (Fig. 5B).

Mechanisms underlying the anti-fibrotic and anti-PH effects of macitentan

Macitentan is blocking both ETA/ETB receptors which mediate ET-1 effects on VSMCs and ECs. *In vitro,* macitentan abolished VSMC contraction and EC death induced by recombinant ET-1 (Supplemental figure 5A-B). Macitentan but not pirfenidone inhibited the contraction of lung fibroblasts induced by rET-1 and also by rTGF-β1 (Fig. 6A; supplemental fig. 5A-B).

As expected, rTGF-β1 induced fibroblast-to-myofibroblast differentiation shown by upregulation of collagen1, α-SMA and TGF-β1 mRNA. Interestingly, macitentan or pirfenidone alone inhibited this upregulation (Fig 6B). The combination of macitentan and pirfenidone showed even lower levels of mRNA for collagen1, α-SMA and TGF-β1 (Fig 6B). The mRNA findings were confirmed at the protein level (Fig. 6B). VEGF and TGF-β1 expression were enhanced in fibroblasts by rTGF-β1 and inhibited by macitentan and pirfenidone (Fig. 6B). In addition, active caspase-3 expression was reduced in fibroblasts that received rTGF-β1 and active caspase-3 levels were restored by macitentan and pirfenidone (Fig. 6B). Interstingly, collagen1A protein expression was strongly reduced by macitentan but not pirfenidone.

Similarly, rTGF-β1 induced mRNA upregulation of collagen1, α-SMA and TGF-β1 in EC suggesting differentiation of EC into myofibroblast-like cells (Fig. 6C). Macitentan alone and in combination with pirfenidone inhibited collagen1, α-SMA and TGF-β1 mRNA upregulation whereas pirfenidone alone had no effect (Fig.6C). Interestingly, VEGF mRNA expression was strongly upregulated by macitentan but not pirfenidone (Fig.6C). At the protein level, α-SMA expression in EC was upregulated by rTGF-β1 and inhibited by macitentan and, to a lesser extent, by pirfenidone (Fig. 6C). Interestingly, VEGF and active caspase-3 regulation in EC was opposite to fibroblasts. In EC, rTGF-β1 induced an increase in caspase-3 and a decrease in VEGF (Fig. 6E) while macitentan, but not pirfenidone, restored VEGF and inhibited caspase-3 expression induced by rTGF-β1 (Fig. 6C). Our results demonstrate that, along with EC apoptosis, ET-1 induces the secretion of latent TGF-β1 and its activation (supplemental figure 5C). Macitentan alone and in combination with pirfenidone inhibited TGF-β1 secretion and activation while pirfenidone alone had no effect (supplemental figure 5C).

In vivo, AdTGF-β1 induced only few caspase-3 positive cells in the parenchyma (fibroblasts) but significant EC apoptosis (supplemental figure 6A). Pirfenidone treated rats had high numbers of caspase-3 positive cells both in parenchyma and endothelium while macitentan alone and combination therapy increased caspase-3 positive cells only in the parenchyma while protecting EC from apoptosis (supplemental figure 6A). Dual fluorescent staining

confirmed that macitentan, pirfenidone and the combination increased caspase-3-positive/α-SMA-positive cells indicating an increase in myofibroblast apoptosis compared to AdTGF-β1 (Fig. 7A). In contrast, AdTGF-β1 induced an increase in caspase-3-positive/CD31-positive cells indicating increased EC apoptosis. Macitentan and the combination therapy but not pirfenidone alone reduced AdTGF-β1 induced EC apoptosis (Fig. 7B).

Discussion

IPF is a progressive disease with poor prognosis and limited therapeutic options. To date only two drugs, nintedanib and pirfenidone [1, 2], affect disease progression and were recently approved for the treatment of IPF. Pulmonary hypertension is a frequent complication of IPF with an incidence of 32% to 73% [15]. The development of PH in IPF is associated with poor prognosis and increased hospitalisation. PH usually develops at advanced stages of IPF, thus, managing PH becomes a valid option to improve patients outcome.

In the current study we show that pulmonary fibrosis mediated by overexpression of active TGF-β1 induces significant PH. Along with an increase in ECM deposition, vascular remodelling was observed in AdTGF-β1 rats with rarefaction of the vasculature, increased vessel wall thickness and EC apoptosis, leading to increased mPAP. Macitentan, a dual endothelin receptor antagonist approved for the treatment of PAH, prevented vascular remodelling and PAH in various animal models [11, 16, 17]. As expected, in our model macitentan counteracted the development of PH induced by AdTGF-β1 as shown by reduced mPAP. Of interest this improvement was associated with an increase in vascular density. Macitentan prevented EC apoptosis promoting the production of VEGF which may be imvolved in vasculature rarefaction. In contrast, pirfenidone showed only moderate effects on PH suggesting a specific effect of macitentan on the vasculature.

In addition, we demonstrate in this study that therapeutic administration of macitentan in fibrotic lungs prevents fibrosis progression. Pirfenidone is an established anti-fibrotic drug that inhibits experimental lung fibrosis [18-20]. The anti-fibrotic efficacy of macitentan was identical to pirfenidone in our model. By D28, collagen deposition in rats receiving macitentan or pirfenidone was reduced compared to rats receiving AdTGF-β1 and no drug. Collagen levels in AdTGF-β1/macitentan or AdTGF-β1/pirfenidone rats at D28 were comparable with the level of AdTGF-β1 rats by D14 suggesting that macitentan and pirfenidone prevented further collagen deposition from D14 to D28 rather than reducing existing fibrosis. The combination of pirfenidone and macitentan did not provide any additional beneficial effect on fibrosis progression compared to monotherapy.

The current paradigm for IPF pathobiology suggests that epithelial micro-injuries of unknown aetiology lead to an increase in pro-fibrotic mediators such as active TGF-β1 which create a pro-fibrotic microenvironment in the lung. The differentiation of fibroblasts into myofibroblasts with the formation of fibroblast foci is a central step promoting production of ECM which disrupt the alveolar architecture [21]. Unlike epithelial/endothelial cells, IPF myofibroblasts are resistant to apoptosis [22]. Pirfenidone inhibits fibroblast to myofibroblast differentiation, ECM production and reduces myofibroblast proliferation *in vitro* and *in vivo* [23, 24]. Our findings confirm that pirfenidone exerts anti-fibrotic effect including inhibition of α-SMA expression in myofibroblasts, TGF-β1 expression and collagen deposition induced by TGF-β1 *in vitro* in fibroblasts and by reducing the pool of myofibroblasts *in vivo* through promoting apoptosis.

It has been demonstrated that ET receptor antagonists ameliorate bleomycin-induced pulmonary fibrosis [8]. Moreover, in a model of systemic sclerosis (SSc), macitentan inhibited the pro-fibrotic myofibroblast phenotype induced by ET-1 in human skin fibroblasts [25]. Circulating or tissue ET-1 levels are upregulated in IPF and SSc patients and in the bleomycin model of pulmonary fibrosis [26-28]. We demonstrate here that macitentan prevents, like pirfenidone, TGF-β1 induced myofibroblast differentiation *in vitro* and induces myofibroblast apoptosis *in vivo*. In our model, both TGF-β1 and ET-1 were upregulated until D28. While macitentan reduced both TGF-β1 and ET-1 levels, pirfenidone inhibited only TGF-β1, suggesting a specific action of macitentan on the ET-1 system. This explains the added benefit of the combination of both on inhibiting fibroblast differentiation *in vitro*. Cipriani *et al.* demonstrated the formation of an ET-1/TGF-β receptor complex in fibroblasts from SSc patients, which highlighted a potential interference between ETR/TGF-β signalling [29]. Therefore, it is not surprising that macitentan, by blocking ET-1 signalling, also inhibits TGF-β1.

The differentiation of EC into myofibroblasts, called endothelial-to-mesenchymal transition (endoMT), is one of the putative sources for myofibroblasts in fibrosis [30]. Here we demonstrated that, in addition to its effect on fibroblast differentiation, macitentan but not pirfenidone inhibits EC differentiation *in vitro* and prevents EC death *in vivo.* EndoMT has also been implicated in the pathogenesis of idiopathic PAH and SSc-PH [31, 32], by promoting vascular remodelling and vasoconstriction. Thus, by inhibiting endoMT and protecting EC from apoptosis, macitentan protects AdTGF-β1 rats from PH and may be protecting AdTGF-β1 rats from subsequent fibrosis while pirfenidone only acts on fibrosis progression. Nevertheless, while endoMT has been demonstrated to promote lung fibrosis in

animal models, the exact contribution of endoMT in human IPF remain elusive and the study of the exact role of macitentan on EC differentiation in IPF requires further inverstigation. Interestingly, it has been demonstrated that EC death induced latent TGF-β1 release in the extracellular compartment and stimulated its activation [33]. Macitentan prevented TGF-β1 release and activation from EC thus limiting AdTGF-β1-induced fibrosis progression in our model.

VEGF is an important contributing factor to both PAH and fibrosis. We have previously demonstrated that VEGF reduces apoptosis of EC, prevents vascular rarefaction, and thereby improves PH [10]. However, augmentation of VEGF expression can also worsen fibrosis [10]. It has been shown that macitentan inhibits VEGF in a model of type 2 diabetes [34]. In our study VEGF expression in whole lungs was upregulated following AdTGF-β1, confirming a putative pro-fibrotic effect of VEGF. VEGF was dramatically reduced by macitentan but not pirfenidone. Still, the reduction of VEGF expression seems conflicting with the vascular protection provided by macitentan. VEGF is a potent cytokine and only little localized presence of VEGF may prove sufficient to exert its angiogenetic properties. Interestingly, after AdTGF-β1 the expression of VEGF in the lung parenchyma was largely increased while it was inhibited around EC. In contrast, macitentan abolished the parenchymal VEGF expression while enhancing its expression in the endothelial layer, which is important considering that VEGF is an important survival signal for EC.

We demonstrate here that pirfenidone exerts its anti-fibrotic action by reducing ECM/TGF-β1 production mainly by inhibiting fibroblast to myofibroblast differentiation and promoting myofibroblast apoptosis. In contrast, macitentan's anti-fibrotic capacity is not limited by its action on fibroblasts.

Our study also confirms previous results showing that circulating ET-1 is upregulated in IPF patients [35] along with ET receptor A. Moreover, we were able to demonstrate a correlation between IPF severity and ET-1 serum level. This supports a potential role for ET-1 blockers in advanced IPF, but these finding need to be confirmed. We strongly believe that this argument holds true even considering that the Macitentan USe in IPF Clinical (MUSIC) trial reported that macitentan was not effective for the treatment of IPF [12]. In our preclinical model, lung fibrosis was correlated with vascular remodelling including endothelial cell death and PH. Signals sent by endothelial cell damage such as latent TGF-β1 release and activation likely worsen fibrosis; a process inhibited by macitentan in rats. While results obtained in preclinical models are certainly not always transposable to humans, we believe that our AdTGF-β1 model may be representative of a specific population of IPF patients with lung

fibrosis and PH which have not been investigated specifically in previous clinical trials. The MUSIC trail, just like the earlier trial investigating the effect of bosentan, another ETA/ETB receptor antagonist, was conducted in patients with mild to moderate IPF who probably did not (yet) have significant remodelling of the pulmonary vasculature and PH [36, 37]. The more recent ARTEMIS trial concluded that ambrisentan, an antagonist selective for the ETA receptor, was not effective in treating IPF and may even be associated with an increased risk for disease progression [38]. Still, ARTEMIS was terminated early, which means that the drug exposure may not have been long enough to see a benefit and only a small fraction of study subjects had group 3 PH (14%) [39]. It is likely that macitentan may have beneficial effect only in a restricted population of IPF patients with advanced disease and PH development which may not have been highlighted in previous clinical trials.

In summary, we demonstrate a solid antifibrotic effect of macitentan on pulmonary fibrosis in a non inflammation driven experimental model of lung fibrosis. The effect is similar to pirfenidone, one of the two approved antifibrotic drugs. In addition, macitentan, alone and in combination with pirfenidone, significantly improved PH and reduced pulmonary vessel remodeling in animals with advanced fibrosis plus PH. These findings strongly support what the investigators of the failed ARTEMIS trials have postulated in their summarizing statement [39]: "*The observations in this limited number of patients with WHO group 3 PH warrant further studies to understand the pathophysiogical aspects and clinical outcomes of the pulmonary vasculopathy associated with IPF*."

Acknowledgments

The authors thank Fuqin Duan for her excellent technical help. We thank Jennifer Wattie and Rod Rhem for their help with the rodent CT scan experiments. We thank Anna Dvorkin-Gheva for her efficient technical help with the Nanostring analysis. Funding for this study was granted by Actelion Pharmaceuticals Ltd. Pierre-Simon Bellaye is funded by le Fonds de Dotation "Recherche en Santé Respiratoire et de la Fondation du Souffle", the Canadian Pulmonary Fibrosis Foundation (CPFF) and the Research institute of St Joseph's Hospital, Hamilton, ON, Canada (FSORC Award). Chiko Shimbori is funded by the Pulmonary Fibrosis Foundation (I.M. Rosenzweig Junior Investigator Award) and Mitacs Canada.

References

1. King TE, Jr., Bradford WZ, Castro-Bernardini S, Fagan EA, Glaspole I, Glassberg MK, Gorina E, Hopkins PM, Kardatzke D, Lancaster L, Lederer DJ, Nathan SD, Pereira CA, Sahn SA, Sussman R, Swigris JJ, Noble PW, Group AS. A phase 3 trial of pirfenidone in patients with idiopathic pulmonary fibrosis. *The New England journal of medicine* 2014: 370(22): 2083-2092.
2. Richeldi L, du Bois RM, Raghu G, Azuma A, Brown KK, Costabel U, Cottin V, Flaherty KR, Hansell DM, Inoue Y, Kim DS, Kolb M, Nicholson AG, Noble PW, Selman M, Taniguchi H, Brun M, Le Maulf F, Girard M, Stowasser S, Schlenker-Herceg R, Disse B, Collard HR, Investigators IT. Efficacy and safety of nintedanib in idiopathic pulmonary fibrosis. *The New England journal of medicine* 2014: 370(22): 2071-2082.
3. Raghu G. Idiopathic Pulmonary Fibrosis: lessons from clinical trials over the past 25 years. *European Respiratory Journal* 2017: 50(4).
4. Blobe GC, Schiemann WP, Lodish HF. Role of transforming growth factor beta in human disease. *The New England journal of medicine* 2000: 342(18): 1350-1358.
5. Patel NM, Lederer DJ, Borczuk AC, Kawut SM. Pulmonary hypertension in idiopathic pulmonary fibrosis. *Chest* 2007: 132(3): 998-1006.
6. Pulido T, Adzerikho I, Channick RN, Delcroix M, Galie N, Ghofrani HA, Jansa P, Jing ZC, Le Brun FO, Mehta S, Mittelholzer CM, Perchenet L, Sastry BK, Sitbon O, Souza R, Torbicki A, Zeng X, Rubin LJ, Simonneau G, Investigators S. Macitentan and morbidity and mortality in pulmonary arterial hypertension. *The New England journal of medicine* 2013: 369(9): 809-818.
7. Elisa T, Antonio P, Giuseppe P, Alessandro B, Giuseppe A, Federico C, Marzia D, Ruggero B, Giacomo M, Andrea O, Daniela R, Mariaelisa R, Claudio L. Endothelin Receptors Expressed by Immune Cells Are Involved in Modulation of Inflammation and in Fibrosis: Relevance to the Pathogenesis of Systemic Sclerosis. *Journal of immunology research* 2015: 2015: 147616.
8. Park SH, Saleh D, Giaid A, Michel RP. Increased endothelin-1 in bleomycin-induced pulmonary fibrosis and the effect of an endothelin receptor antagonist. *American journal of respiratory and critical care medicine* 1997: 156(2 Pt 1): 600-608.
9. Shi-Wen X, Chen Y, Denton CP, Eastwood M, Renzoni EA, Bou-Gharios G, Pearson JD, Dashwood M, du Bois RM, Black CM, Leask A, Abraham DJ. Endothelin-1 promotes myofibroblast induction through the ETA receptor via a rac/phosphoinositide 3-kinase/Akt-dependent pathway and is essential for the enhanced contractile phenotype of fibrotic fibroblasts. *Molecular biology of the cell* 2004: 15(6): 2707-2719.
10. Farkas L, Farkas D, Ask K, Moller A, Gauldie J, Margetts P, Inman M, Kolb M. VEGF ameliorates pulmonary hypertension through inhibition of endothelial apoptosis in experimental lung fibrosis in rats. *J Clin Invest* 2009: 119(5): 1298-1311.
11. Iglarz M, Steiner P, Wanner D, Rey M, Hess P, Clozel M. Vascular Effects of Endothelin Receptor Antagonists Depends on Their Selectivity for ETA Versus ETB Receptors and on the Functionality of Endothelial ETB Receptors. *Journal of cardiovascular pharmacology* 2015: 66(4): 332-337.
12. Raghu G, Million-Rousseau R, Morganti A, Perchenet L, Behr J, Group MS. Macitentan for the treatment of idiopathic pulmonary fibrosis: the randomised controlled MUSIC trial. *The European respiratory journal* 2013: 42(6): 1622-1632.
13. Ask K, Bonniaud P, Maass K, Eickelberg O, Margetts PJ, Warburton D, Groffen J, Gauldie J, Kolb M. Progressive pulmonary fibrosis is mediated by TGF-beta isoform 1 but not TGF-beta3. *The international journal of biochemistry & cell biology* 2008: 40(3): 484-495.
14. Hubner RH, Gitter W, El Mokhtari NE, Mathiak M, Both M, Bolte H, Freitag-Wolf S, Bewig B. Standardized quantification of pulmonary fibrosis in histological samples. *BioTechniques* 2008: 44(4): 507-511, 514-507.
15. Shorr AF, Wainright JL, Cors CS, Lettieri CJ, Nathan SD. Pulmonary hypertension in patients with pulmonary fibrosis awaiting lung transplant. *The European respiratory journal* 2007: 30(4): 715-721.

16. Temple IP, Monfredi O, Quigley G, Schneider H, Zi M, Cartwright EJ, Boyett MR, Mahadevan VS, Hart G. Macitentan treatment retards the progression of established pulmonary arterial hypertension in an animal model. *International journal of cardiology* 2014: 177(2): 423-428.
17. Iglarz M, Landskroner K, Bauer Y, Vercauteren M, Rey M, Renault B, Studer R, Vezzali E, Freti D, Hadana H, Schlapfer M, Cattaneo C, Bortolamiol C, Weber E, Whitby BR, Delahaye S, Wanner D, Steiner P, Nayler O, Hess P, Clozel M. Comparison of Macitentan and Bosentan on Right Ventricular Remodeling in a Rat Model of Non-vasoreactive Pulmonary Hypertension. *Journal of cardiovascular pharmacology* 2015: 66(5): 457-467.
18. Inomata M, Kamio K, Azuma A, Matsuda K, Kokuho N, Miura Y, Hayashi H, Nei T, Fujita K, Saito Y, Gemma A. Pirfenidone inhibits fibrocyte accumulation in the lungs in bleomycin-induced murine pulmonary fibrosis. *Respiratory research* 2014: 15: 16.
19. Kakugawa T, Mukae H, Hayashi T, Ishii H, Abe K, Fujii T, Oku H, Miyazaki M, Kadota J, Kohno S. Pirfenidone attenuates expression of HSP47 in murine bleomycin-induced pulmonary fibrosis. *The European respiratory journal* 2004: 24(1): 57-65.
20. Antoniu SA. Pirfenidone for the treatment of idiopathic pulmonary fibrosis. *Expert opinion on investigational drugs* 2006: 15(7): 823-828.
21. Barkauskas CE, Noble PW. Cellular mechanisms of tissue fibrosis. 7. New insights into the cellular mechanisms of pulmonary fibrosis. *American journal of physiology Cell physiology* 2014: 306(11): C987-996.
22. Thannickal VJ, Horowitz JC. Evolving concepts of apoptosis in idiopathic pulmonary fibrosis. *Proc Am Thorac Soc* 2006: 3(4): 350-356.
23. Shin JM, Park JH, Park IH, Lee HM. Pirfenidone inhibits transforming growth factor beta1-induced extracellular matrix production in nasal polyp-derived fibroblasts. *American journal of rhinology & allergy* 2015: 29(6): 408-413.
24. Lehtonen ST, Veijola A, Karvonen H, Lappi-Blanco E, Sormunen R, Korpela S, Zagai U, Skold MC, Kaarteenaho R. Pirfenidone and nintedanib modulate properties of fibroblasts and myofibroblasts in idiopathic pulmonary fibrosis. *Respiratory research* 2016: 17: 14.
25. Cutolo M, Montagna P, Brizzolara R, Smith V, Alessandri E, Villaggio B, Sulli A, Tavilla PP, Pizzorni C, Soldano S. Effects of macitentan and its active metabolite on cultured human systemic sclerosis and control skin fibroblasts. *The Journal of rheumatology* 2015: 42(3): 456-463.
26. Cambrey AD, Harrison NK, Dawes KE, Southcott AM, Black CM, du Bois RM, Laurent GJ, McAnulty RJ. Increased levels of endothelin-1 in bronchoalveolar lavage fluid from patients with systemic sclerosis contribute to fibroblast mitogenic activity in vitro. *American journal of respiratory cell and molecular biology* 1994: 11(4): 439-445.
27. Uguccioni M, Pulsatelli L, Grigolo B, Facchini A, Fasano L, Cinti C, Fabbri M, Gasbarrini G, Meliconi R. Endothelin-1 in idiopathic pulmonary fibrosis. *Journal of clinical pathology* 1995: 48(4): 330-334.
28. Mutsaers SE, Foster ML, Chambers RC, Laurent GJ, McAnulty RJ. Increased endothelin-1 and its localization during the development of bleomycin-induced pulmonary fibrosis in rats. *American journal of respiratory cell and molecular biology* 1998: 18(5): 611-619.
29. Cipriani P, Di Benedetto P, Ruscitti P, Verzella D, Fischietti M, Zazzeroni F, Liakouli V, Carubbi F, Berardicurti O, Alesse E, Giacomelli R. Macitentan inhibits the transforming growth factor-beta profibrotic action, blocking the signaling mediated by the ETR/TbetaRI complex in systemic sclerosis dermal fibroblasts. *Arthritis research & therapy* 2015: 17: 247.
30. Piera-Velazquez S, Mendoza FA, Jimenez SA. Endothelial to Mesenchymal Transition (EndoMT) in the Pathogenesis of Human Fibrotic Diseases. *Journal of clinical medicine* 2016: 5(4).
31. Good RB, Gilbane AJ, Trinder SL, Denton CP, Coghlan G, Abraham DJ, Holmes AM. Endothelial to Mesenchymal Transition Contributes to Endothelial Dysfunction in Pulmonary Arterial Hypertension. *The American journal of pathology* 2015: 185(7): 1850-1858.
32. Ranchoux B, Antigny F, Rucker-Martin C, Hautefort A, Pechoux C, Bogaard HJ, Dorfmuller P, Remy S, Lecerf F, Plante S, Chat S, Fadel E, Houssaini A, Anegon I, Adnot S, Simonneau G, Humbert M,

Cohen-Kaminsky S, Perros F. Endothelial-to-mesenchymal transition in pulmonary hypertension. *Circulation* 2015: 131(11): 1006-1018.
33. Sakao S, Taraseviciene-Stewart L, Wood K, Cool CD, Voelkel NF. Apoptosis of pulmonary microvascular endothelial cells stimulates vascular smooth muscle cell growth. *American journal of physiology Lung cellular and molecular physiology* 2006: 291(3): L362-368.
34. Sen S, Chen S, Feng B, Iglarz M, Chakrabarti S. Renal, retinal and cardiac changes in type 2 diabetes are attenuated by macitentan, a dual endothelin receptor antagonist. *Life sciences* 2012: 91(13-14): 658-668.
35. Barlo NP, van Moorsel CH, Kazemier KM, van den Bosch JM, Grutters JC. Potential role of endothelin-1 in pulmonary fibrosis: from the bench to the clinic. *American journal of respiratory cell and molecular biology* 2010: 42(5): 633.
36. King TE, Jr., Behr J, Brown KK, du Bois RM, Lancaster L, de Andrade JA, Stahler G, Leconte I, Roux S, Raghu G. BUILD-1: a randomized placebo-controlled trial of bosentan in idiopathic pulmonary fibrosis. *American journal of respiratory and critical care medicine* 2008: 177(1): 75-81.
37. King TE, Jr., Brown KK, Raghu G, du Bois RM, Lynch DA, Martinez F, Valeyre D, Leconte I, Morganti A, Roux S, Behr J. BUILD-3: a randomized, controlled trial of bosentan in idiopathic pulmonary fibrosis. *American journal of respiratory and critical care medicine* 2011: 184(1): 92-99.
38. Raghu G, Behr J, Brown KK, Egan JJ, Kawut SM, Flaherty KR, Martinez FJ, Nathan SD, Wells AU, Collard HR, Costabel U, Richeldi L, de Andrade J, Khalil N, Morrison LD, Lederer DJ, Shao L, Li X, Pedersen PS, Montgomery AB, Chien JW, O'Riordan TG, Investigators* A-I. Treatment of idiopathic pulmonary fibrosis with ambrisentan: a parallel, randomized trial. *Annals of internal medicine* 2013: 158(9): 641-649.
39. Raghu G, Nathan SD, Behr J, Brown KK, Egan JJ, Kawut SM, Flaherty KR, Martinez FJ, Wells AU, Shao L, Zhou H, Henig N, Szwarcberg J, Gillies H, Montgomery AB, O'Riordan TG. Pulmonary hypertension in idiopathic pulmonary fibrosis with mild-to-moderate restriction. *The European respiratory journal* 2015: 46(5): 1370-1377.

Figure legends

Figure 1. *The ET-1 system is activated in IPF patients.*

A. ET-1 protein level measured by ELISA in serum from healthy controls (n=9) and IPF patients (n=31), results are presented as mediane with interquartile range; *p < 0.05. **B.** Correlation between ET-1 level in sera of IPF patients and % predicted FVC (left) and % predicted TLC (right). **C.** IHC staining for ET receptor A on tissue from control and IPF patients with moderate and advanced IPF. Representative images and quantification of staining made with the ImageJ software are shown, results are presented as mediane with interquartile range; *p < 0.05, **p < 0.01, n = 6 per group. **D.** IHC staining for ET receptor B on tissue from control and IPF patients with moderate and advanced IPF. Representative images and quantification of staining made with the ImageJ software are shown, results are presented as mediane with interquartile range; n = 6 per group.

Figure 2. *Macitentan but not pirfenidone is preventing PH induced by TGF-β1.*

A. Mean pulmonary artery pressure measured at time of sacrifice. mPAP is expressed in mmHg and as mediane with interquartile range; *p < 0.05, **p < 0.01, ***p < 0.001, ns = non-significant, n = 5 for AdDL D28/AdTGF-β1 D14/AdTGF-β1 D21/AdTGF-β1 pirfenidone D28/AdTGF-β1 Macitentan D28, n = 6 for AdTGF-β1 Pirf + Maci D28 and n = 9 for AdTGF-β1 D28. **B.** ET-1 protein level measured by ELISA in serum and BAL, mediane with interquartile range; **p < 0.01, *p < 0.05, ns = non-significant, n = 5 for AdDL D28/AdTGF-β1 D14/AdTGF-β1 D21/AdTGF-β1 D28/AdTGF-β1 pirfenidone D28/AdTGF-β1 Macitentan D28, n = 6 for AdTGF-β1 Pirf + Maci D28. **C.** Representative image of CT scans of the vasculature of AdTGF-β1 (AdDL as control), AdTGF-β1 + macitentan, AdTGF-β1 + pirfenidone or AdTGF-β1 +macitentan + pirfenidone rats at D28 obtained from AMIRA software. **D.** Vascular density and vascular volumes calculated from CT scans of vasculature of AdTGF-β1 (AdDL as control), AdTGF-β1 + macitentan, AdTGF-β1 + pirfenidone or AdTGF-β1 +macitentan + pirfenidone rats; mean ± SEM; *p < 0.05, n = 6 per group for AdDL and AdTGF-β1 and n = 5 per group for AdTGF-β1 + macitentan, AdTGF-β1 + pirfenidone or AdTGF-β1 +macitentan + pirfenidone.

Figure 3. *Macitentan but not pirfenidone is modulating VEGF expression in AdTGF-β1 treated rats.*

A. ET-1 protein level measured by ELISA in Serum and BAL, mediane with interquartile range; **p < 0.01, n = 5 for AdDL D28/AdTGF-β1 D14/AdTGF-β1 D21/AdTGF-β1

D28/AdTGF-β1 pirfenidone D28/AdTGF-β1 Macitentan D28, n = 6 for AdTGF-β1 Pirf + Maci D28 . **B.** VEGF expression measured by western blot in whole lung lysates of AdTGF-β1 (AdDL as control), AdTGF-β1 + macitentan, AdTGF-β1 + pirfenidone or AdTGF-β1 +macitentan + pirfenidone rats. GAPDH was used as loading control. Relative intensity of VEGF expression was normalized with GAPDH using ImageJ; mediane with interquartile range, n = 4 per group. **C.** Representative image of IHC of VEGF on AdTGF-β1 (AdDL as control), AdTGF-β1 + macitentan, AdTGF-β1 + pirfenidone or AdTGF-β1 +macitentan + pirfenidone rats at D28. Upper panel shows representative parenchymal area. Lower panel shows representative vessels, Black arrows show VEGF-positive endothelial cells.

Figure 4. *Macitentan and pirfenidone prevent the progression of AdTGF-β1 induced lung fibrosis.*

A. Hydroxyproline measurements on whole lung lysates of AdTGF-β1 (AdDL as control), AdTGF-β1 + macitentan, AdTGF-β1 + pirfenidone or AdTGF-β1 +macitentan + pirfenidone rats; mediane with interquartile range; **p < 0.01, n = 5 for AdDL D28/AdTGF-β1 D14/AdTGF-β1 D21/AdTGF-β1 D28/AdTGF-β1 pirfenidone D28/AdTGF-β1 Macitentan D28, n = 6 for AdTGF-β1 Pirf + Maci D28. **B.** Ashcroft scoring (left panel) and assessment of percentage of fibrotic area (right panel) on lung sections stained by Masson trichrome from AdTGF-β1 (AdDL as control), AdTGF-β1 + macitentan, AdTGF-β1 + pirfenidone or AdTGF-β1 +macitentan + pirfenidone rats; mediane with interquartile range; *p<0.01, **p < 0.01, n = 5 for AdDL D28/AdTGF-β1 D14/AdTGF-β1 D21/AdTGF-β1 D28/AdTGF-β1 pirfenidone D28/AdTGF-β1 Macitentan D28, n = 6 for AdTGF-β1 Pirf + Maci D28. **C.** Representative lung sections stained by Masson trichrome from AdTGF-β1 (AdDL as control), AdTGF-β1 + macitentan, AdTGF-β1 + pirfenidone or AdTGF-β1 +macitentan + pirfenidone rats at D28 and imaged by slide scanner. **D.** (upper panel) Lung collagen quantification using Pico-Sirus Red (PSR) intensity measurements on lung section from AdTGF-β1 (AdDL as control), AdTGF-β1 + macitentan, AdTGF-β1 + pirfenidone or AdTGF-β1 +macitentan + pirfenidone rats; mediane with interquartile range; **p < 0.01, *p < 0.05, n = 5 for AdDL D28/AdTGF-β1 D14/AdTGF-β1 D21/AdTGF-β1 D28/AdTGF-β1 pirfenidone D28/AdTGF-β1 Macitentan D28, n = 6 for AdTGF-β1 Pirf + Maci D28. (lower panel) Representative lung sections stained by PSR from AdTGF-β1 (AdDL as control), AdTGF-β1 + macitentan, AdTGF-β1 + pirfenidone or AdTGF-β1 +macitentan + pirfenidone rats at D28 and imaged by slide scanner.

Figure 5. *Macitentan and pirfenidone inhibit pro-fibrotic pathways in vivo in AdTGF-β1 rats.* **A.** Total and Active TGF-β1 protein level measured by ELISA in BAL of AdTGF-β1 (AdDL as control), AdTGF-β1 + macitentan, AdTGF-β1 + pirfenidone or AdTGF-β1 +macitentan + pirfenidone rats, mediane with interquartile range; ***p < 0.001, **p < 0.01, *p<0.05, n = 5 for AdDL D28/AdTGF-β1 D14/AdTGF-β1 D21/AdTGF-β1 D28/AdTGF-β1 pirfenidone D28/AdTGF-β1 Macitentan D28, n = 6 for AdTGF-β1 Pirf + Maci D28. **B.** p-Smad3, Smad3, ET-1, α-SMA, ETRA and ETRB expression measured by western blot in whole lung lysates of AdTGF-β1 (AdDL as control), AdTGF-β1 + macitentan, AdTGF-β1 + pirfenidone or AdTGF-β1 +macitentan + pirfenidone rats. GAPDH was used as loading control. Relative intensity of was normalized with GAPDH using ImageJ; mediane with interquartile range; ***p < 0.001, **p < 0.01, *p < 0.05, n = 6 per group.

Figure 6. *Macitentan induces myofibroblasts apoptosis and protects endothelial cells in vitro.* **A.** Control human fibroblasts mixed in a collagen gel cultured in 24 well plates for 12 hours in medium without FBS. After 12 hours cells are treated with TGF-β1 (5 ng/ml) and macitentan (100 µM), pirfenidone (100 µM) or the combination for 24 hours. After 24 hours gels were released for the edge of each well and gel contraction was measured every 2 hours. Graphs show contraction index (mm) at 36 hours and evolution of contraction from 0 to 36 hours after gel release; mediane with interquartile range, *p < 0.05, n = 5. Pictures show representative gel contraction at 0h and 36h. **B.** (left panel) mRNA expression of TGF-β1, Collagen1A, Acta2 and VEGF in human control fibroblasts 24h after treatment with rTGF-β1 (5 ng/ml) and macitentan (100 µM), pirfenidone (100 µM) or the combination, mediane with interquartile range, ***p < 0.001, **p < 0.01, n = 6. (right panel) Expression of α-SMA, TGF-β1, Collagen1A, cleaved caspase-3 (cCasp-3) and VEGF in human control fibroblasts analyzed by western blot 48h after treatment with rTGF-β1 (5 ng/ml) and macitentan (100 µM), pirfenidone (100 µM) or the combination. GAPDH was used as loading control. **C.** (left panel) mRNA expression of TGF-β1, Collagen1A, VEGF and Acta2 in human pulmonary artery endothelial cells 24h after treatment with rTGF-β1 (5 ng/ml) and macitentan (100 µM), pirfenidone (100 µM) or the combination, mediane with interquartile range, ***p < 0.001, **p < 0.01, *p < 0.05, ns = non-significant, n = 6. (right panel) Expression of α-SMA, TGF-β1, Collagen1A, cleaved caspase-3 (cCasp-3) and VEGF in human pulmonary artery endothelial cells analyzed by western blot 48h after treatment with rTGF-β1 (5 ng/ml) and macitentan (100 µM), pirfenidone (100 µM) or the combination. GAPDH was used as loading control.

Figure 7. *Macitentan induces myofibroblasts apoptosis and protects endothelial cells in vivo.* **A.** Representative image of dual immunofluorescent staining of α-SMA (Green), cleaved caspase-3 (Red) on lung section from rats treated with AdTGF-β1 (AdDL as control), AdTGF-β1 + macitentan, AdTGF-β1 + pirfenidone or AdTGF-β1 +macitentan + pirfenidone at D28. DAPI was used a nuclear marker. White arrows show α-SMA+/caspase-3+ cells. **B.** Representative image of dual immunofluorescent staining of CD31 (Green), cleaved caspase-3 (Red) on lung section from rats treated with AdTGF-β1 (AdDL as control), AdTGF-β1 + macitentan, AdTGF-β1 + pirfenidone or AdTGF-β1 +macitentan + pirfenidone at D28. DAPI was used a nuclear marker. White arrows show CD31+/caspase-3+ cells.

Figure 1

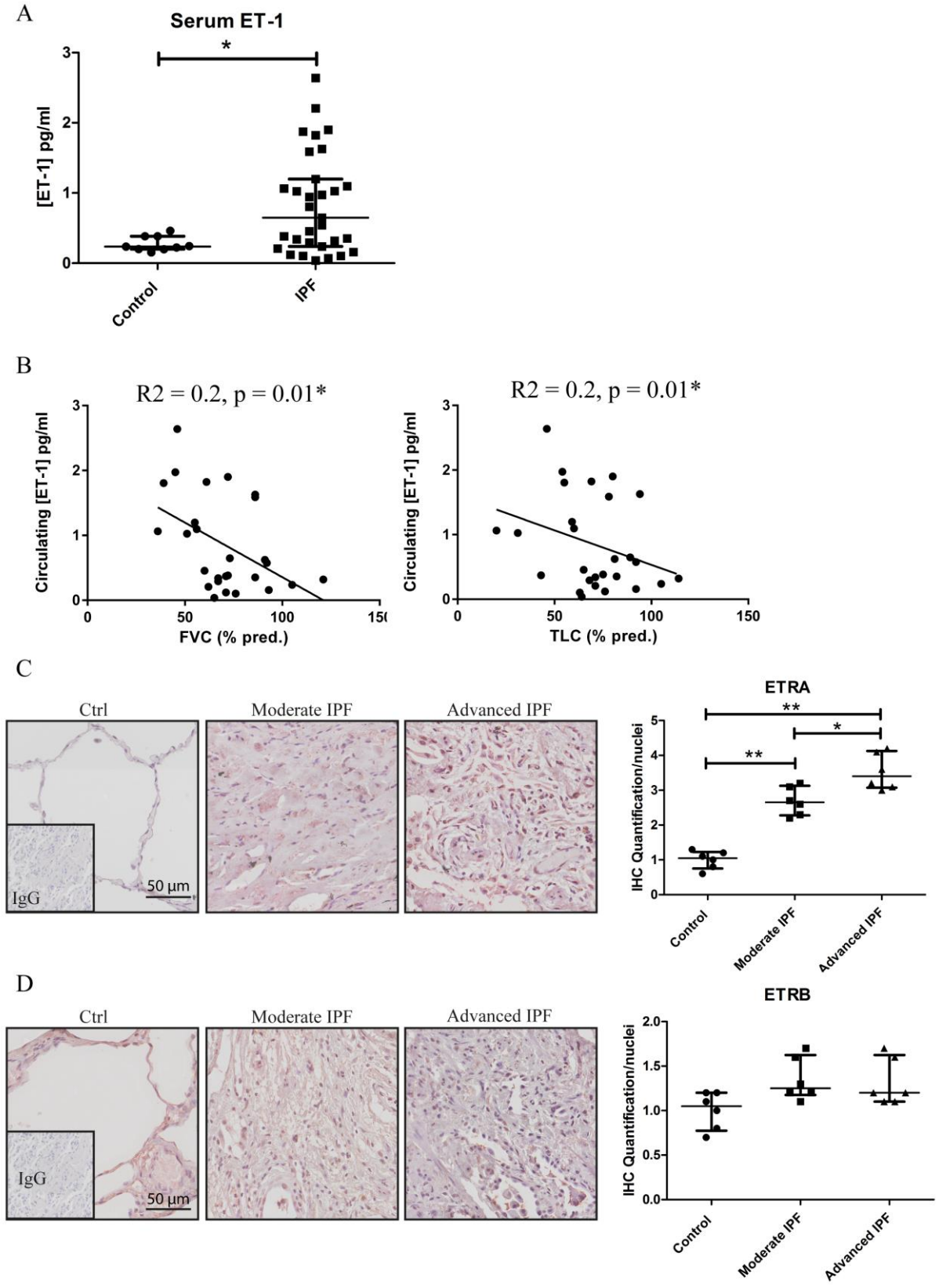
A
Serum ET-1
*
[ET-1] pg/ml
Control
IPF
B
R2 = 0.2, p = 0.01*
Circulating [ET-1] pg/ml
FVC (% pred.)
R2 = 0.2, p = 0.01*
Circulating [ET-1] pg/ml
TLC (% pred.)
C
Ctrl
Moderate IPF
Advanced IPF
IgG
50 µm
ETRA
IHC Quantification/nuclei
Control
Moderate IPF
Advanced IPF
D
Ctrl
Moderate IPF
Advanced IPF
IgG
50 µm
ETRB
IHC Quantification/nuclei
Control
Moderate IPF
Advanced IPF

Figure 2

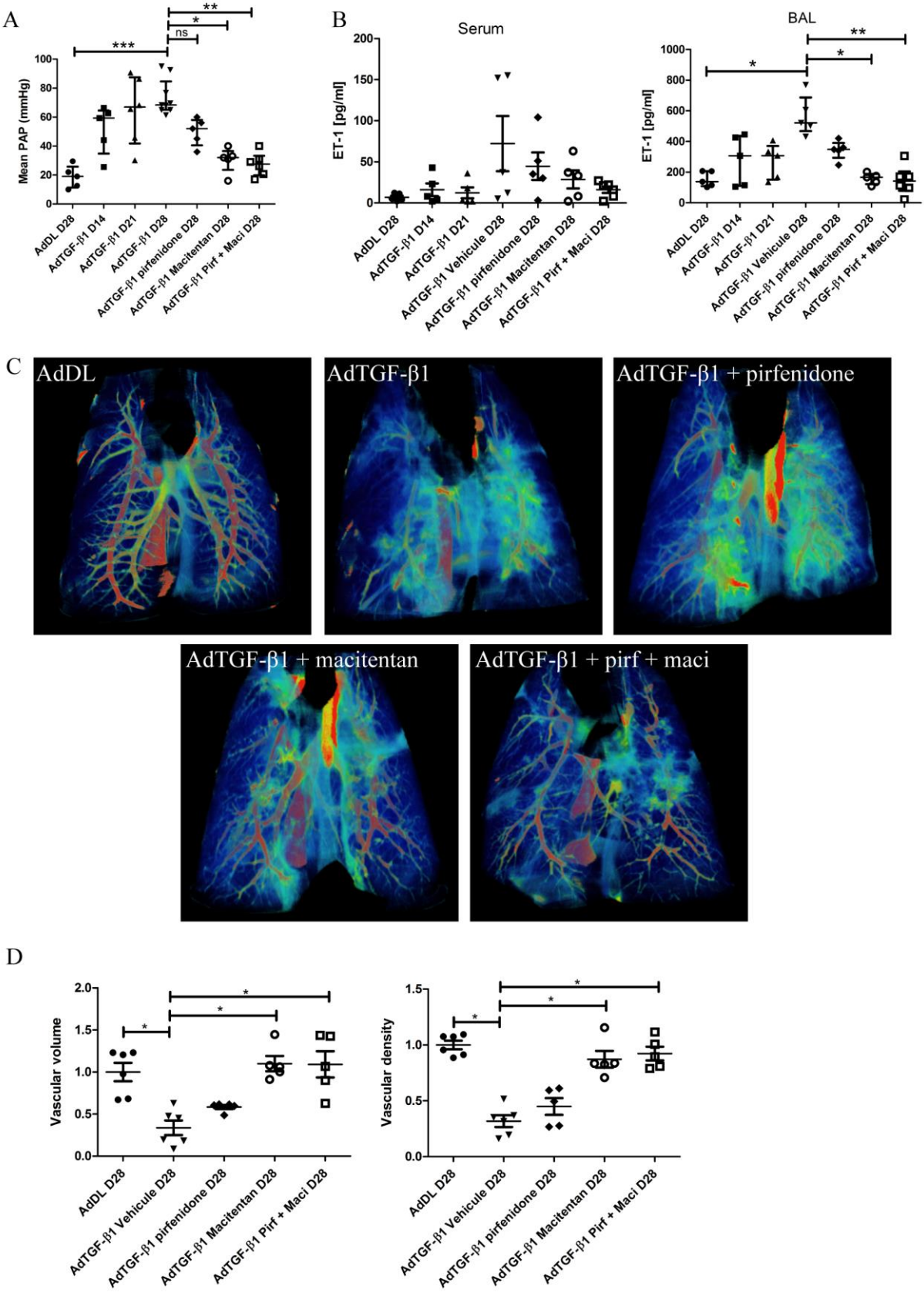
A
Mean PAP (mmHg)
***
*
ns
**
AdDL D28
AdTGF-β1 D14
AdTGF-β1 D21
AdTGF-β1 D28
AdTGF-β1 pirfenidone D28
AdTGF-β1 Macitentan D28
AdTGF-β1 Pirf + Maci D28
B
Serum
ET-1 [pg/ml]
AdTGF-β1 Vehicule D28
BAL
C
AdDL
AdTGF-β1
AdTGF-β1 + pirfenidone
AdTGF-β1 + macitentan
AdTGF-β1 + pirf + maci
D
Vascular volume
Vascular density

Figure 3

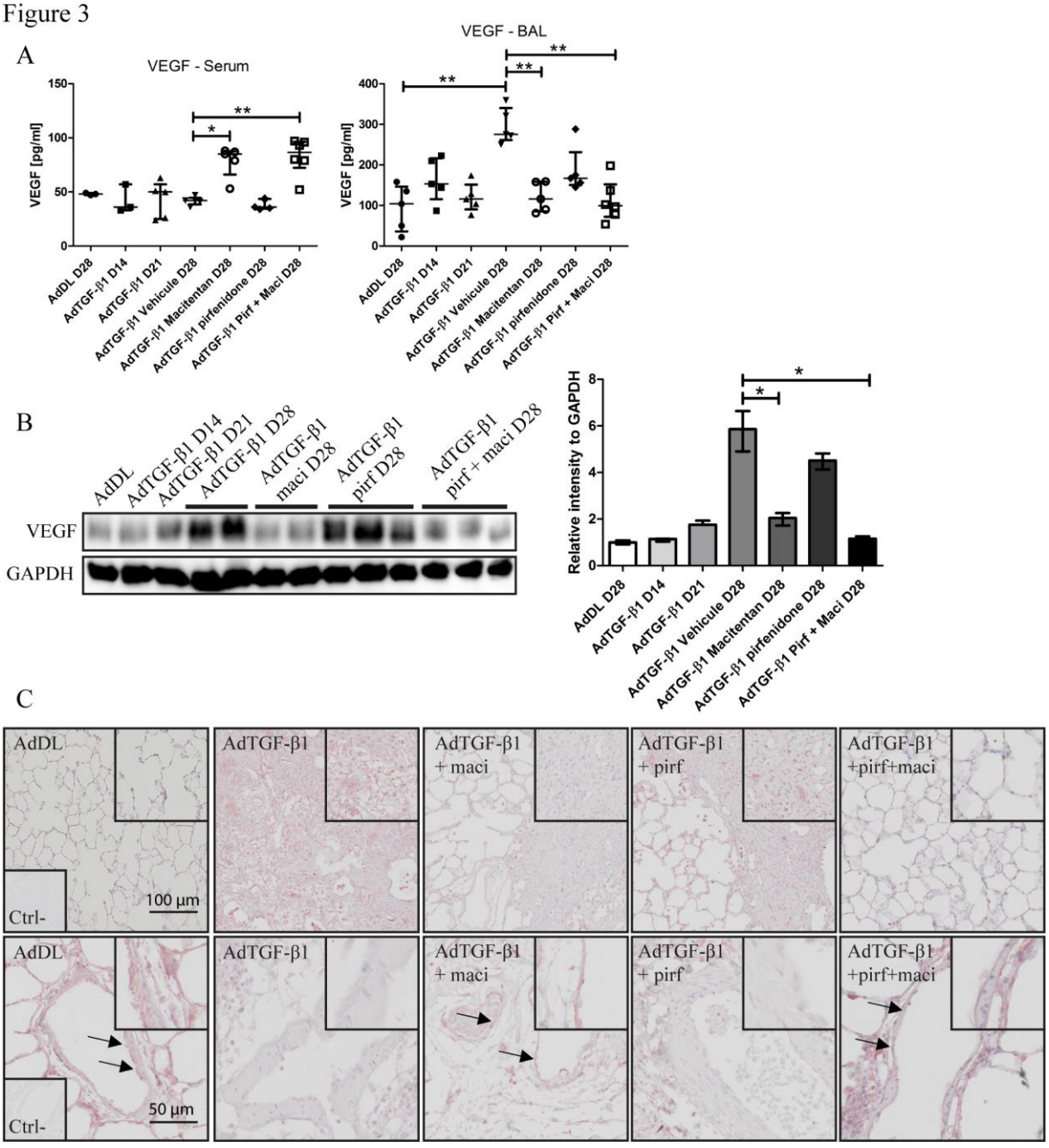
A
VEGF - Serum
VEGF [pg/ml]
VEGF - BAL
AdDL D28
AdTGF-β1 D14
AdTGF-β1 D21
AdTGF-β1 Vehicule D28
AdTGF-β1 Macitentan D28
AdTGF-β1 pirfenidone D28
AdTGF-β1 Pirf + Maci D28
B
AdDL
AdTGF-β1 D14
AdTGF-β1 D21
AdTGF-β1 D28
AdTGF-β1 maci D28
AdTGF-β1 pirf D28
AdTGF-β1 pirf + maci D28
VEGF
GAPDH
Relative intensity to GAPDH
C
AdDL
AdTGF-β1
AdTGF-β1 + maci
AdTGF-β1 + pirf
AdTGF-β1 +pirf+maci
Ctrl-
100 µm
50 µm

Figure 4

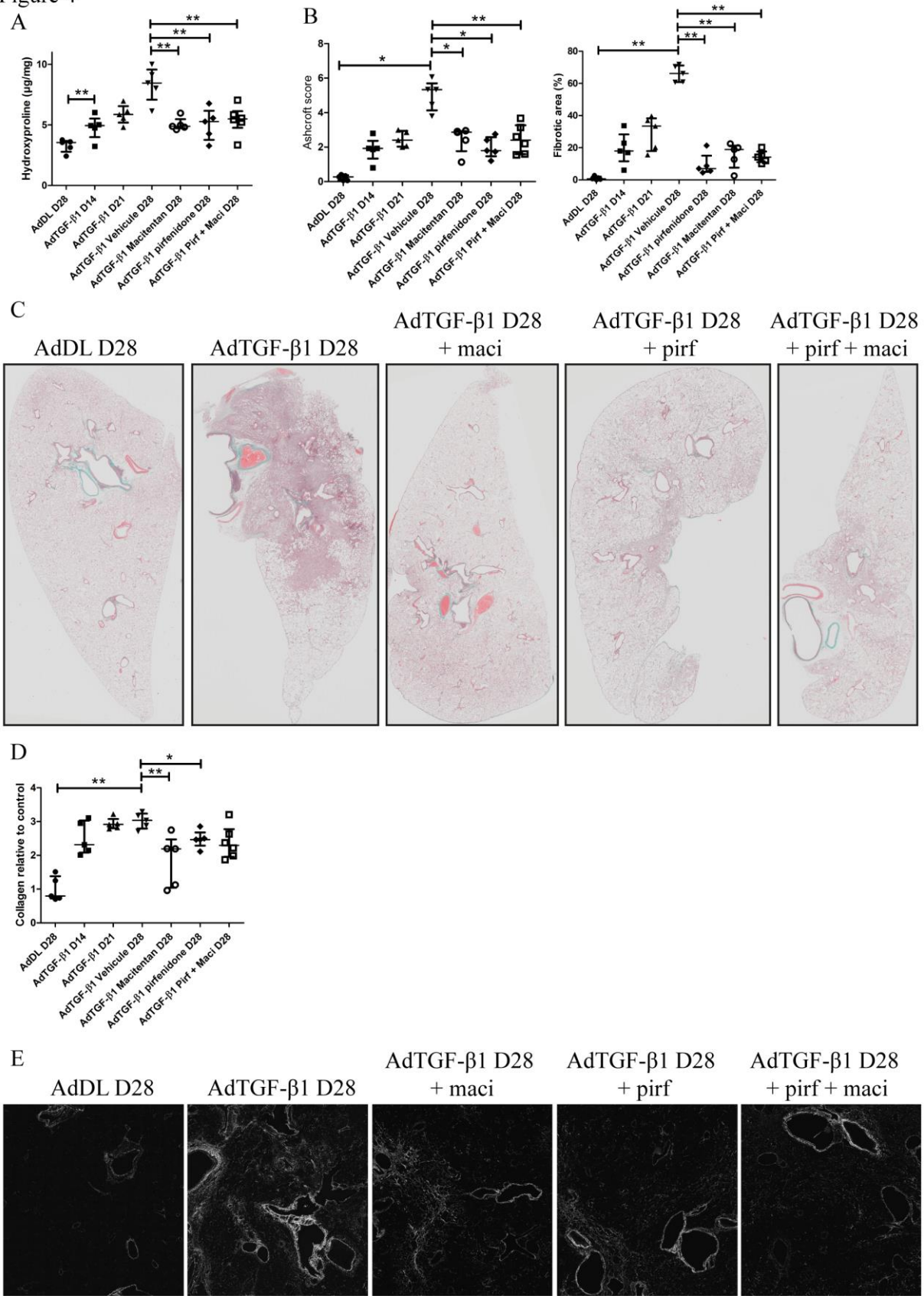
A
Hydroxyproline (µg/mg)
B
Ashcroft score
Fibrotic area (%)
AdDL D28
AdTGF-β1 D14
AdTGF-β1 D21
AdTGF-β1 Vehicule D28
AdTGF-β1 Macitentan D28
AdTGF-β1 pirfenidone D28
AdTGF-β1 Pirf + Maci D28
C
AdDL D28
AdTGF-β1 D28
AdTGF-β1 D28 + maci
AdTGF-β1 D28 + pirf
AdTGF-β1 D28 + pirf + maci
D
Collagen relative to control
E
AdDL D28
AdTGF-β1 D28
AdTGF-β1 D28 + maci
AdTGF-β1 D28 + pirf
AdTGF-β1 D28 + pirf + maci

Figure 5

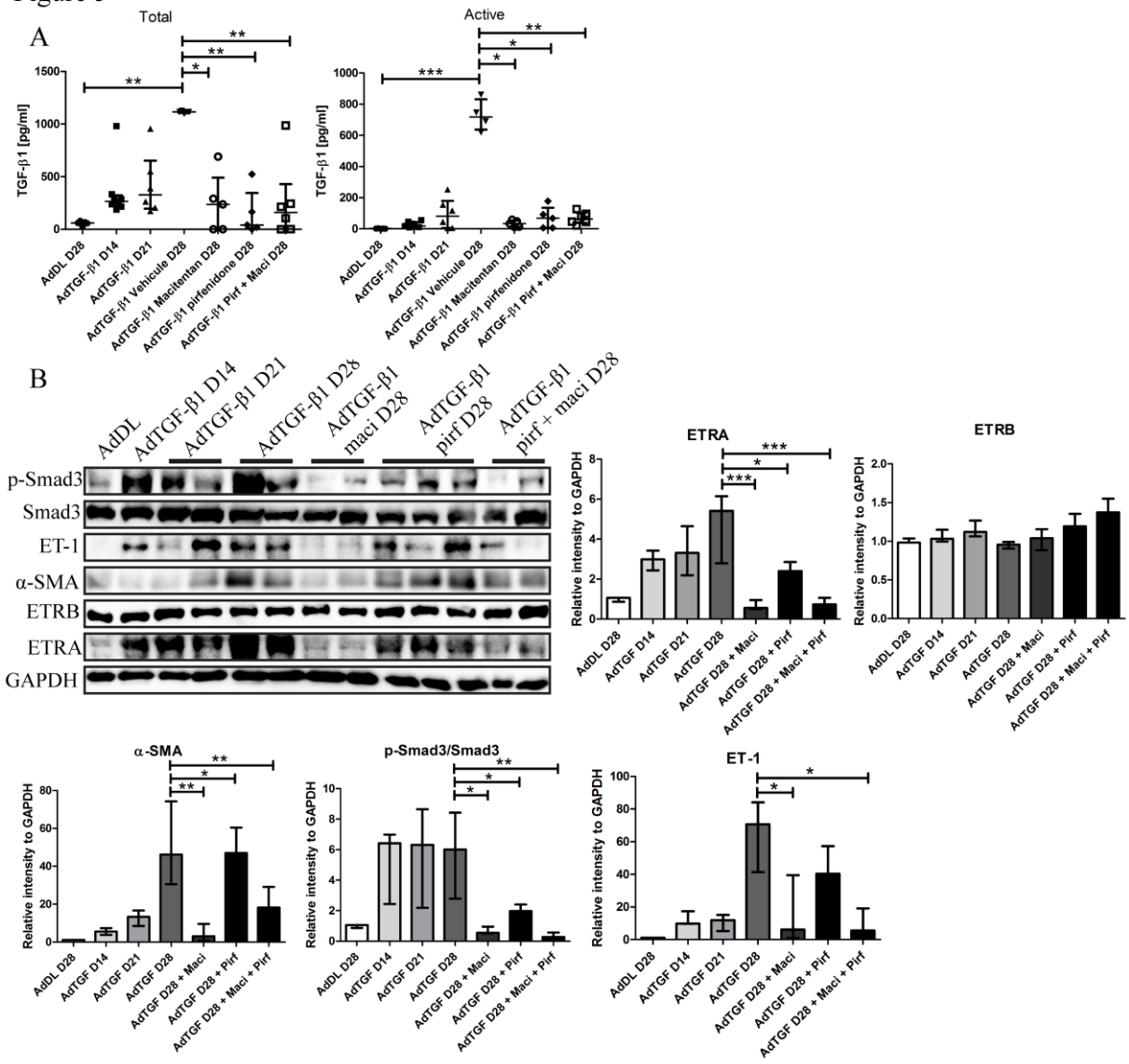
A
Total
Active
TGF-β1 [pg/ml]
AdDL D28
AdTGF-β1 D14
AdTGF-β1 D21
AdTGF-β1 Vehicule D28
AdTGF-β1 Macitentan D28
AdTGF-β1 pirfenidone D28
AdTGF-β1 Pirf + Maci D28
B
AdDL
AdTGF-β1 D14
AdTGF-β1 D21
AdTGF-β1 D28
AdTGF-β1 maci D28
AdTGF-β1 pirf D28
AdTGF-β1 pirf + maci D28
p-Smad3
Smad3
ET-1
α-SMA
ETRB
ETRA
GAPDH
ETRA
ETRB
α-SMA
p-Smad3/Smad3
ET-1
Relative intensity to GAPDH
AdDL D28
AdTGF D14
AdTGF D21
AdTGF D28
AdTGF D28 + Maci
AdTGF D28 + Pirf
AdTGF D28 + Maci + Pirf

Figure 6

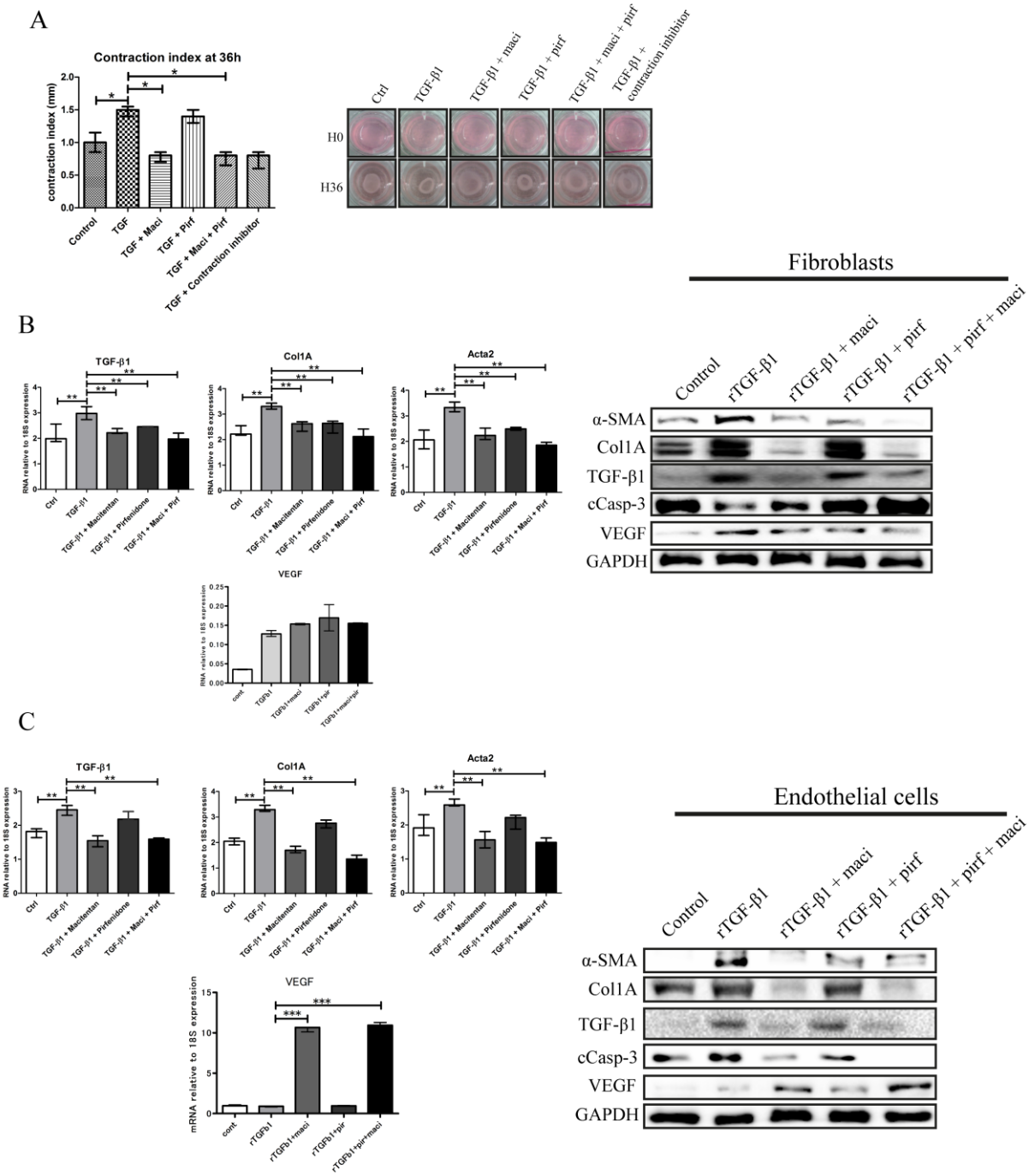
A
Contraction index at 36h
contraction index (mm)
Control
TGF
TGF + Maci
TGF + Pirf
TGF + Maci + Pirf
TGF + Contraction inhibitor
Ctrl
TGF-β1
TGF-β1 + maci
TGF-β1 + pirf
TGF-β1 + maci + pirf
TGF-β1 + contraction inhibitor
H0
H36
B
TGF-β1
Col1A
Acta2
VEGF
RNA relative to 18S expression
Ctrl
TGF-β1
TGF-β1 + Macitentan
TGF-β1 + Pirfenidone
TGF-β1 + Maci + Pirf
Fibroblasts
Control
rTGF-β1
rTGF-β1 + maci
rTGF-β1 + pirf
rTGF-β1 + pirf + maci
α-SMA
Col1A
TGF-β1
cCasp-3
VEGF
GAPDH
C
TGF-β1
Col1A
Acta2
VEGF
mRNA relative to 18S expression
cont
rTGFb1
rTGFb1+maci
rTGFb1+pir
rTGFb1+pir+maci
Endothelial cells
Control
rTGF-β1
rTGF-β1 + maci
rTGF-β1 + pirf
rTGF-β1 + pirf + maci
α-SMA
Col1A
TGF-β1
cCasp-3
VEGF
GAPDH

Figure 7

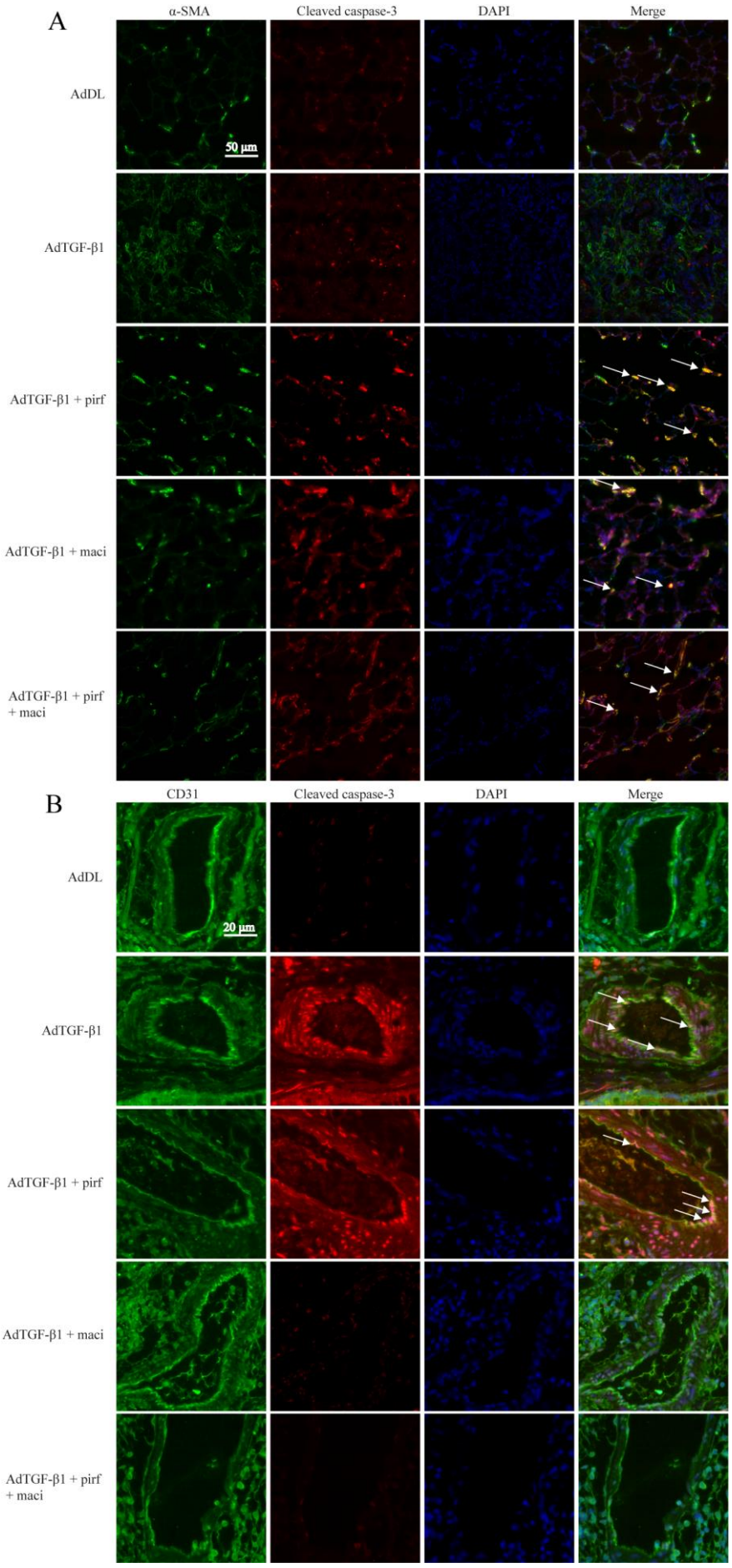
A
α-SMA
Cleaved caspase-3
DAPI
Merge
AdDL
50 μm
AdTGF-β1
AdTGF-β1 + pirf
AdTGF-β1 + maci
AdTGF-β1 + pirf + maci
B
CD31
Cleaved caspase-3
DAPI
Merge
AdDL
20 μm
AdTGF-β1
AdTGF-β1 + pirf
AdTGF-β1 + maci
AdTGF-β1 + pirf + maci

Online supplemental Materials and Methods

Human samples

All sera and tissue were collected with patient consent in compliance with the Research Ethics Board of St. Joseph's Healthcare Hamilton. Hamilton Integrated Research Ethics Board (HIREB #00-1839) approval was obtained prior to beginning the study. Aged matched healthy volunteers were used as controls. Peripheral blood was collected from healthy volunteers or confirmed IPF patients and sera were aliquoted and stored at -80°C. The biopsies analysed in this study revealed a usual interstitial pneumonia (UIP) pattern on histopathology. Non-fibrotic human lungs were used as control. Following biopsy, all tissue was fixed in 10% neutral-buffered formalin and embedded in paraffin. Patient were classified as "moderate" or "advanced" based on pulmonary function tests and a FVC threshold of 50–55% predicted was used to separate moderate patients from those with severe disease as previously described [1].

Antibodies and reagents

Antibodies are α-smooth muscle actin (α-SMA) (ab7817, Abcam), pSmad3 (ab51451, Abcam), Smad3 (ab40854, Abcam), VEGF (ab1316, Abcam), Cleaved caspase-3 (#9661, cell signaling), ET-1 (ab117757, Abcam), CD31 (sc-1506, Santacruz biotech.), ETRA (ab117521, Abcam), ETRB (ab117529, Abcam), GAPDH (#5174, Cell signaling technology). Anti-rabbit HRP linked IgG (#7074, Cell Signaling Technology), Anti-mouse IgG HRP-linked Antibody (#7076, Cell Signaling Technology). For fluorescence microscopy, we used goat or donkey secondary antibody conjugated with Alexa Fluor-488 and Alexa Fluor-555 (Abcam). Human rET-1 (100-21, PerproTech) and human rTGF-β1 (240-B, R&D systems).

Cell culture

Human derived normal primary pulmonary artery smooth muscle cells (ATCC, PCS-100-023) were grown in Vascular Cell Basal Medium (ATCC, PCS-100-030) with Vascular Smooth Muscle Cell Growth Kit components (ATCC, PCS-100-042). Human derived normal primary pulmonary artery endothelial cells (ATCC, PCS-100-022) were grown in Vascular Cell Basal Medium (ATCC, PCS-100-030) with the Endothelial Cell Growth Kit-BBE (ATCC, PCS-100-040). Fibroblast cells were obtained from humans during surgical biopsy (control and IPF) and grown in RPMI medium (ATCC, 30-2001) supplemented with 10% FBS and 1% pen-strep (ATCC). All cells were incubated at 37°C, 5% CO^2 and grown in T75 Falcon flasks. All cells were used at passages between P2 and P8.

Animal Experiments

Pulmonary fibrosis was induced by an adenoviral gene vector encoding biologically active TGF-β1 (AdTGF-β1). Female Sprague-Dawley rats (225–250 g; Charles River, Wilmington, MA) received 5.0 x 10^8 PFU of AdTGF-β1 by single intratracheal instillation under isoflurane anesthesia at D0. Control animals received an empty vector construct (AdDL). Rats received either macitentan (Actelion pharmaceuticals Ltd., Switzerland), pirfenidone (Chemcia Scientific, USA) either a combination of both (n=6 animal per group). Pirfenidone (0.5% food admix, ad libitum), macitentan (daily gavage 100 mg/kg/d) and corresponding vehicles (Gelatin 7.5% in water) were given from day 14 to day 28. Rats were sacrificed at day 14, 21 or 28 and bronchoalveolar lavage (BALF), blood and lung tissue was harvested. Before sacrifice, rats were anesthetised with ketamine/xylazine (Xylazine (Bayer Healthcare, 10 mg/kg) and ketamine (150 mg/kg)) and a plastic catheter (PE tubing, SP0109, ADInstruments Inc, USA) was introduced in the jugular vein of the rats up to the right ventricle of the heart. The catheter was then pushed further into the pulmonary artery. The catheter was linked to a pressure transducer (MLT844, ADInstruments Inc, USA) and an analysis system (PowerLab 4/35, LabChart Pro, ADInstruments Inc, USA) in order to record the mean pulmonary artery pressure (PAP). Rats were left untouched for at least 2 minutes before the measurements in order to record a stable value of PAP. After the measurement, an incision was made in the femoral artery and lungs were harvested and either fixed in 10% formalin for histology or flash frozen in liquid nitrogen for protein and RNA analysis.

All animal work was conducted under the guidelines from the Canadian Council on Animal Care and approved by the Animal Research Ethics Board of McMaster University under protocol #13-12-48.

CT scans imaging

Rats were sedated via an intraperitoneal injection of Xylazine (Bayer Healthcare, 10 mg/kg) and ketamine (150 mg/kg). After exposing a section of the anterior side of the neck a 16-gauge needle was inserted into the jugular vein and contrast agent (Isovue-300 (iopamidol injection), 0270-1315-25, Bracco Diagnostics Canada Inc., Mississauga, Ont. Canada) was perfused for at least 10 minutes (0.2 mm/minutes). An incision was made in the femoral artery to bleed the animal. Once contrast agent had perfused the entire vascular of the animal, rats were placed in the CT scan machine and imaged (n=3). All imaging work was completed at the McMaster Centre for Preclinical and Translational Imaging (MCPTI) at McMaster

University (Hamilton, ON, Canada). The CT scan was acquired on an X-SPECT system (Gamma Medica, Northridge,CA, USA) and consisted of 1024 X-ray projections with x-ray tube characteristics of 75 kVp and 355 μA. The projection images were reconstructed using a Feldkamp cone beam backprojection algorithm in COBRA (Exxim Sofware, Pleasanton, CA, USA) into 512×512×512 arrays (0.1 mm isotropic voxels). Each CT image was converted to Hounsfield Unit (HU) scaling using empty airspace within the field of view and a water-filled tube included in each scan. Images were analysed with the AMIRA software (FEI Visualization Sciences Group, USA). The 3D reconstruction of the pulmonary arterial tree was achieved with multiple steps. The total chest space volume, excluding the heart, was selected using a combination of manual segmentation and semi-automated contouring. Threshold segmentation identified the vascular tree and was optimized for each image. Due to voxel size accurate segmentation and subsequent quantification could only be performed on vessels larger the 75 μm. Data provided segment volume and density.

Western blotting

Crushed lungs were homogenized in cell lysis buffer (Hepes 50 mM pH7.4, Nacl 150 mM, EDTA 5 mM, Triton X-100 0.5%) using a mechanical homogenizer (Omni International, Waterbuy CT), and the collected supernatant was used for western blotting. 40 μg of total protein from lung homogenate or cells were separated on a 10% SDS Polyacrylamide Electrophoresis gels. Proteins were transferred to a PVDF membrane (Bio-Rad Laboratories, 1620177, Hercules, CA) using a wet transfer apparatus and blocked at room temperature for 1 hour using 8% skim milk. Western blotting assay was used to detect α-SMA, pSmad3, Smad3, VEGF, ET-1, ETRA and ETRB. GAPDH wass used as loading control. Protein detection was performed using the SuperSignal West Pico chemiluminescent system (Thermo Fischer Scientific, 34580) and read in a ChemiDoc XRS Imaging System (Bio-Rad Laboratories). Densitometry measurements were performed with ChemiDoc XRS Imaging System Software and were normalized to a control sample when studies required more than one blot.

Hydroxyproline assay

Hydroxyproline content in rat lung tissue was measured by a colorimetric assay as described previously [2]. Briefly, lung lobes were turned into a finely ground up powder and immediately homogenized in RIPA buffer. The total pellet formed from the centrifugation of the RIPA homogenized lung tissues was resuspended in PBS and allowed to freeze at -80°C.

The pellet was then subsequently lyophilized for at least 24 hours using a freezer dryer apparatus (Modulyod Freezer Dryer, Thermo Electron Corporation). Following the addition of 10% TCA solution and subsequent centrifugation, 6ml of 6N HCL were added into each tube for pellet hydrolysis at 110°C in dry bath incubator. Samples were later brought to a pH of 7 by the addition of NaOH and were incubated for 20 minutes after the addition of 0.05M Chloramine T reagent. Chloramine T reagent was destroyed by the adding 70% perchloric acid and samples were ultimately incubated for 20 minutes in a 55-65°C water bath shortly after adding Ehrlich's reagent solution. The final reaction absorbance was read at 550nm and samples concentrations were determined from the hydroxyproline standard curve. Hydroxyproline concentrations were finally calculated and expressed as microgram of hydroxyproline per ml of solution.

Ashcroft score

Pulmonary fibrosis of Masson Trichrome stained lung sections was graded from 0 (normal lung) to 8 (completely fibrotic lung), using a modified Ashcroft score [3].

Isolation of mRNA and gene expression

Total RNA was extracted from frozen lung tissue with TRIzol® reagent (Thermo fisher scientific, 15596026). Two μg of total RNA was reverse transcribed using qScript cDNA Super Mix (Quanta Bioscience, 95048-025, Gaithersburg, MD). The cDNA was amplified using a Fast 7500 real-time PCR system (AB Applied Biosystems) using TaqMan® Universal PCR Master Mix and predesigned primer pairs (Life Technologies, 4304437, Burlington, ON, Canada) for Collagen1A (Hs00164004_m1), TGFβR1 (Hs00610320_m1), ACTA2 (Hs00426835_g1) and 18S (Hs03003631_g1).

Histology and immunohistochemistry

Lungs were fixed by intratracheal instillation of 10% neutral-buffered formalin at a pressure of 20 cm H_2O. Paraffin sections were cut at 4 μm and processed in-house at the core histology facility at McMaster (Hamilton, ON, Canada). Tissue slides were generated and subsequent staining was performed with Masson Trichrome (MT) or Picrosirius Red (PSR). Picture acquisition of PSR and MT staining were performed using an Automatic slide scanner microscope (Olympus VS 120-L). PSR quantification was performed on whole lung sections using the ImageJ software (NIH, USA). Endothelial Diameter (ED) was defined as distance between external elastic laminae, while Medial Wall Thickness (MWT) was determined as

distance between external and internal elastic laminae. Vessels were categorized as follows: Small: ED < 50 µm and large: ED > 50 µm. MWT was calculated using the following formula: MWT (%) = (2 × MT/ED) × 100%. The number of vessels was evaluated in histological sections using ImageJ. Briefly, lung slides pictures were converted in TIFF and 20 random fields were chosen per pictures and the number of small and large vessels were manually evaluated using ImageJ in each field (using a straight line of 50µm in imageJ to determine the size of the vessels > or < to 50µm).

This automatic slide scanner can digitalize whole slides at 20X magnifications using polarized detection. Immunohistochemical staining was performed to characterize the localization and expression of VEGF (ab1316, Abcam). Images were captured using an automatic slide scanner microscope (Olympus VS 120-L). All sections were digitalized at 20X from 4 transverse sections and quantitated by ImageJ automatic analysis, excluding the main bronchus and larger airways. Images were analysed using an internally developed macro on ImageJ. The macro was created to threshold and quantify the amount of staining and could subsequently be used to determine total tissue area within a region of interest (ROI). Olympus vsi. files were extracted using the BIOP plugin on ImageJ and converted to tiff. files. The images were then edited in Adobe Photoshop to remove any debris surrounding the tissue sample as to minimize extraneous detection of undesired particulates. Next, the macro was run and set to threshold and display a specific hue (H), saturation (S), and brightness (B) range (specific values were then determined for ETRA, ETRB and VEGF staining) using the Colour Threshold plugin. Once thresholding was applied to only display the desired H, S, and B ranges, images were converted into 8-bit images. The analyse particle function was then used to determine the total area of the stained regions. Specific H, S, and B values to quantify total tissue area were then used. Finding the total stained area, and the total tissue area, a proportion of the sample which was stained could be determined.

The fibrotic area on lung slices was evaluated using an in-house macro for ImageJ. Briefly, the macro opened a .tiff image in ImageJ and allowed successive manual drawing of total lung area and fibrotic area. The macro automatically calculated total lung area and fibrotic area and results were expressed as % of fibrotic area compared with total lung area.

Immunofluorescence

Immunostaining of VEGF and α-SMA was performed on formalin fixed rat lung tissues sections. Briefly, following deparaffinization and saturation of nonspecific sites with BSA (5%, 30 min), cells were incubated with primary antibodies overnight in a humidified

chamber at 4°C. Conjugated secondary antibodies were used at a dilution of 1:2000. Slides were mounted in Prolong-gold with DAPI (ProLong® Gold antifade regent with DAPI, Life technologies, P36931). Pictures were taken were performed using an Automatic slide scanner microscope (Olympus VS 120-L).

ELISA

The levels of active TGF-β1, VEGF and ET-1 in rat and human BALF supernatants and sera were measured using a rat TGF-β1-specific ELISA kit (MB100B , R&D Systems), a rat VEGF ELISA kit (abcam, ab100786), a rat ET-1 ELISA kit (E-EL-R0167, Elabscience) and a human ET-1 ELISA kit (R&D Systems, DET100) respectively, according to the manufacturer's recommendations.

Contraction assay

Collagen gel solution was made at the bottom of a 24 well following the manufacturer's recommendations (CBA-201, Cell BioLabs, Inc.).

Human derived pulmonary fibroblasts or pulmonary artery smooth muscle cells (5 x 10^6 cells/mL) were mixed with the collagen gel solution and seeded onto the 24 well plate. This mix was then incubated for 1-hour at 37°C to allow it to set. After 1-hour 1mL of respective medium was carefully added onto the now set gel solution and then incubated overnight at 37°C, 5% CO^2. The following day the medium was changed and the cells in the gel were treated with vehicle (DMSO), rTGF-β1 (5ng/ml, PerproTech, 100-21) or rET-1 (10 µM, Abcam, ab158332) and Macitentan (100µM), pirfenidone (100µM) or both. A control well was treated with rTGF-β1 (5ng/ml, PerproTech, 100-21) and a contraction inhibitor provided by the manufacturer. Cells were incubated at 37°C, 5% CO^2 for 24 more hours to allow for stress to develop. Gels were released from the slides of the wells to allow contraction to occur. This was accomplished by running a scalpel along the perimeter of the wells. Gels were measured prior to release, and every 1 hour after release for 6 hours. Measurements were then repeated every 12 hours for the next 48 hours.

Flow cytometry

Endothelial cell apoptosis has been assessed via Annexin-V/PI staining using a Annexin V-FITC Apoptosis Detection Kit (ab14085, Abcam) according to manufacturer recommendation. Analysis has been perform using a FACS CANTO flow cytometer (BD Biosciences) and FlowJo software.

Statistical Analysis

All data were expressed as mediane with interquartile range. Statistical analysis between two groups was performed using a non-parametric Mann-Whitney test. Statistical analysis between multiple groups with one control group was performed by Kruskal-Wallis test, with Dunn comparison test (post hoc). Analysis was performed with GraphPad Prism 6.0 (GraphPad Software Inc.). A p-value less than 0.05 was considered significant.

1. Kolb M, Collard HR. Staging of idiopathic pulmonary fibrosis: past, present and future. *European respiratory review : an official journal of the European Respiratory Society* 2014: 23(132): 220-224.
2. Ask K, Bonniaud P, Maass K, Eickelberg O, Margetts PJ, Warburton D, Groffen J, Gauldie J, Kolb M. Progressive pulmonary fibrosis is mediated by TGF-beta isoform 1 but not TGF-beta3. *The international journal of biochemistry & cell biology* 2008: 40(3): 484-495.
3. Hubner RH, Gitter W, El Mokhtari NE, Mathiak M, Both M, Bolte H, Freitag-Wolf S, Bewig B. Standardized quantification of pulmonary fibrosis in histological samples. *BioTechniques* 2008: 44(4): 507-511, 514-507.

Supplemental Figure 1.

A. Count of blood vessels (small < 50 µm; large > 50 µm) performed on Masson trichrome stained lung sections from AdTGF-β1 (AdDL as control), AdTGF-β1 + macitentan, AdTGF-β1 + pirfenidone or AdTGF-β1 +macitentan + pirfenidone rats at D28; mediane with interquartile range, ***p < 0.001, **p < 0.01, *p < 0.05, n = 6 per group. **B.** Representative images of pulmonary blood vessels stained with Masson trichrome from AdTGF-β1 (AdDL as control), AdTGF-β1 + macitentan, AdTGF-β1 + pirfenidone or AdTGF-β1 +macitentan + pirfenidone rats at D28. **C.** Medial wall thickness (MWT, small < 50 µm; large > 50 µm) measured with ImageJ on lung sections from AdTGF-β1 (AdDL as control), AdTGF-β1 + macitentan, AdTGF-β1 + pirfenidone or AdTGF-β1 +macitentan + pirfenidone rats at D28; mediane with interquartile range, ***p < 0.001, *p < 0.05, n = 6 per group.

Supplemental Figure 2.

A. Representative image of IHC of VEGF on AdTGF-β1 (AdDL as control), AdTGF-β1 + macitentan, AdTGF-β1 + pirfenidone or AdTGF-β1 +macitentan + pirfenidone rats at D28. Upper panel shows representative parenchymal area. Lower panel shows representative vessels.

Supplemental Figure 3.

A. Representative image of immunofluorescence of VEGF and CD31 on AdTGF-β1 (AdDL as control), AdTGF-β1 + macitentan, AdTGF-β1 + pirfenidone or AdTGF-β1 +macitentan + pirfenidone rats at D28. Panel shows representative parenchymal area. CD31 = green, VEGF = red, DAPI = Blue. **B.** Representative image of immunofluorescence of VEGF and CD31 on AdTGF-β1 (AdDL as control), AdTGF-β1 + macitentan, AdTGF-β1 + pirfenidone or AdTGF-β1 +macitentan + pirfenidone rats at D28. Panel shows representative vessels. CD31 = green, VEGF = red, DAPI = Blue.

Supplemental Figure 4.

A. Lung fonction measured by Flexivent. Pressure-Volume loops are presented for AdTGF-β1 (AdDL as control), AdTGF-β1 + macitentan, AdTGF-β1 + pirfenidone or AdTGF-β1 +macitentan + pirfenidone rats at D28. **p < 0.01, *p < 0.05, n = 4 per group. B. Quantification and representative images of CT scan 3D reconstruction of fibrotic area (blue) and healthy parenchyma (red) of AdTGF-β1 (AdDL as control), AdTGF-β1 + macitentan,

AdTGF-β1 + pirfenidone or AdTGF-β1 +macitentan + pirfenidone rats at D28, *p < 0.05, n = 3 per group.

Supplemental Figure 5.

A. Human pulmonary artery endothelial cells (upper panel) or control human fibroblasts (lower panel) mixed in a collagen gel cultured in 24 well plates for 12 hours in medium without FBS. After 12 hours cells are treated with ET-1 (10 µM) and macitentan (100 µM), pirfenidone (100 µM) or the combination for 24 hours. After 24 hours gels were released for the edge of each well and gel contraction was measured every 2 hours. Graphs show contraction index (mm) at 36 hours and evolution of contraction from 0 to 36 hours after gel release; mediane with interquartile range, *p < 0.05, n = 5. Pictures show representative gel contraction at 0h and 36h. **B.** Apoptosis measured using AnnexinV/PI staining. Percentage of viable cells (AnnexinV-/PI-), early apoptotic cells (AnnexinV+/PI-) and late apoptotic cells (AnnexinV+/PI+) was measured by flow cytometry, mediane with interquartile range, **p < 0.01, *p<0.05, n = 5. **C.** Total and Active TGF-β1 protein level measured by ELISA in EC supernantants after ET-1, ET-1 + macitentan, ET-1 + pirfenidone or ET-1 +macitentan + pirfenidone, mediane with interquartile range; *p < 0.05, **p < 0.01, n = 5 per group.

Supplemental Figure 6.

A. Representative image of immunochemistry staining of cleaved caspase-3 (brown) on lung section from rats treated with AdTGF-β1 (AdDL as control), AdTGF-β1 + macitentan, AdTGF-β1 + pirfenidone or AdTGF-β1 +macitentan + pirfenidone at D28. Upper panel shows representative parenchymal area. Lower panel shows representative blood vessel area. Black arrows show caspase-3+ cells.

Supplemental Figure 1

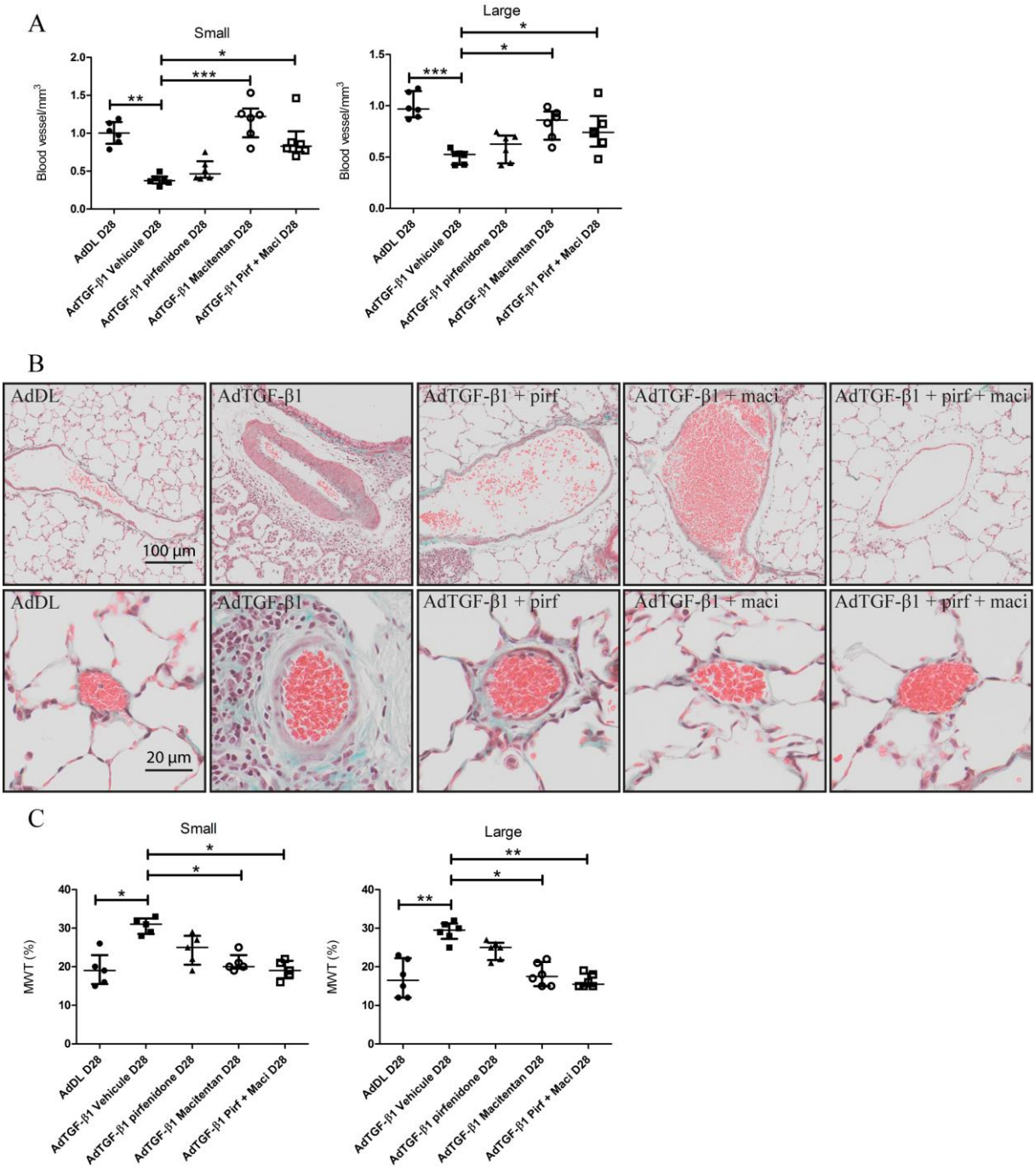

Supplemental Figure 2

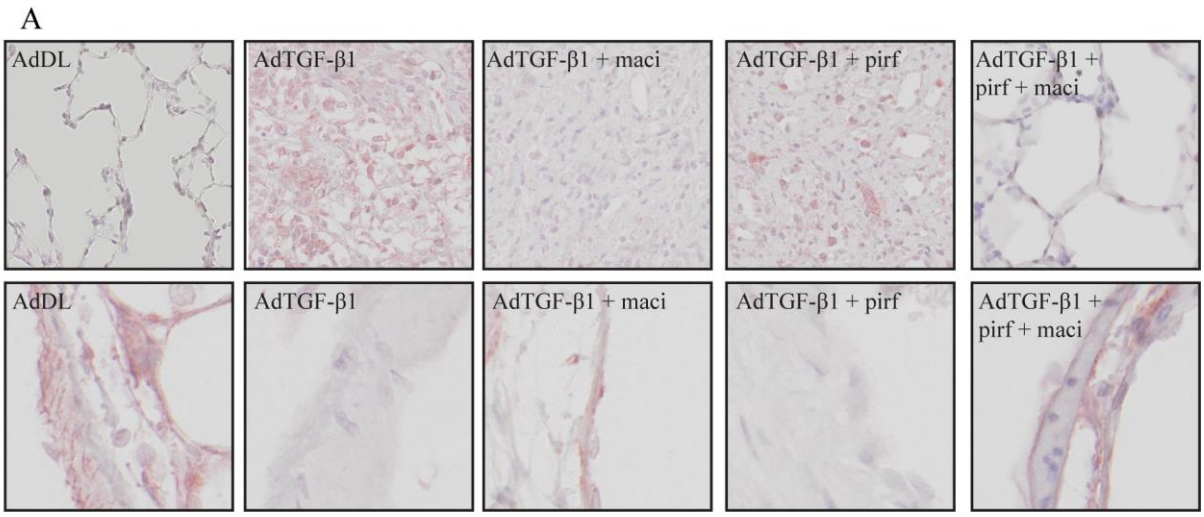

Supplemental Figure 3

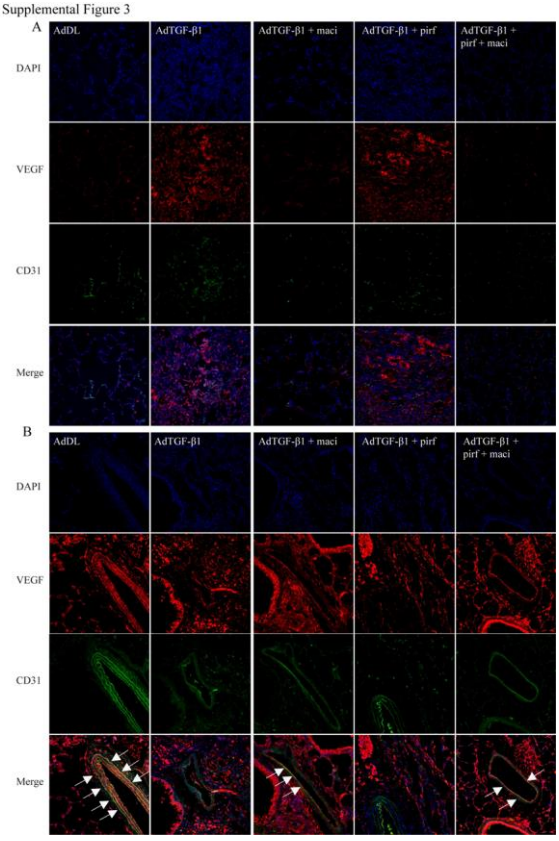

Supplemental Figure 4

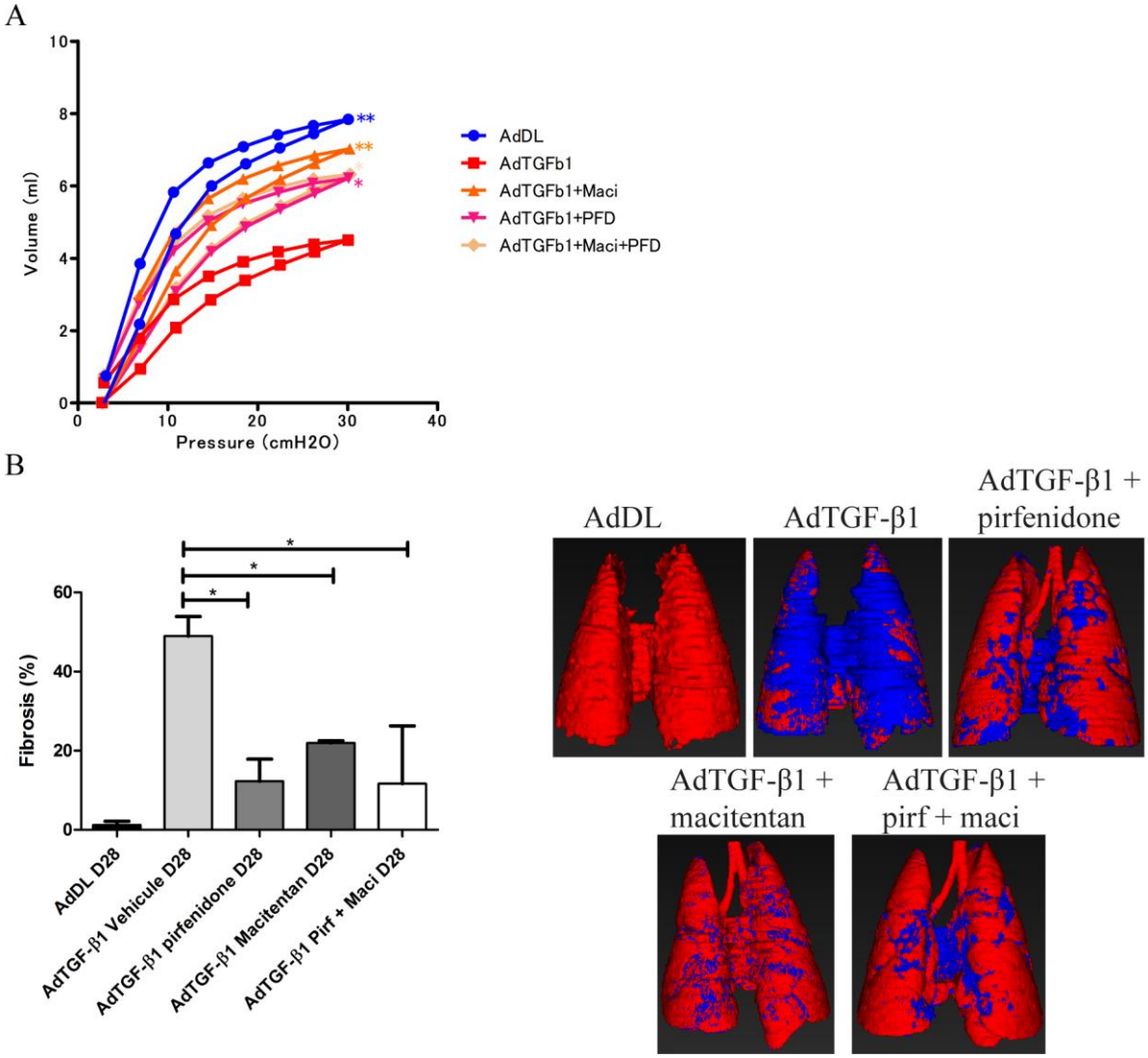

Supplemental Figure 5

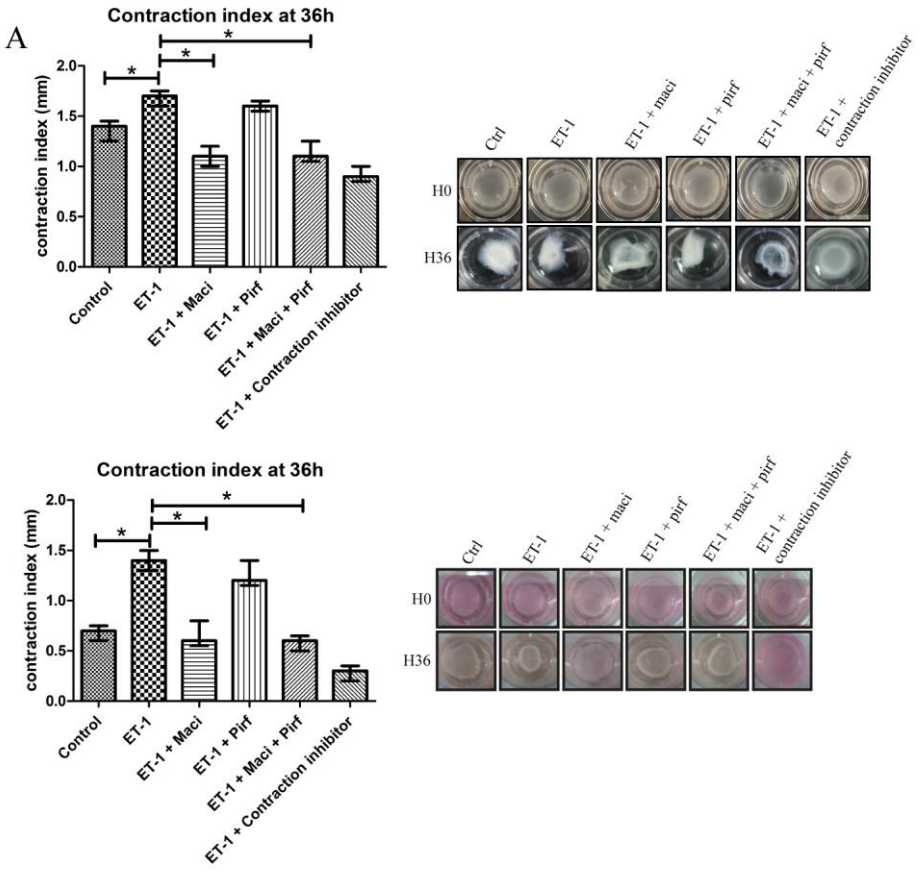

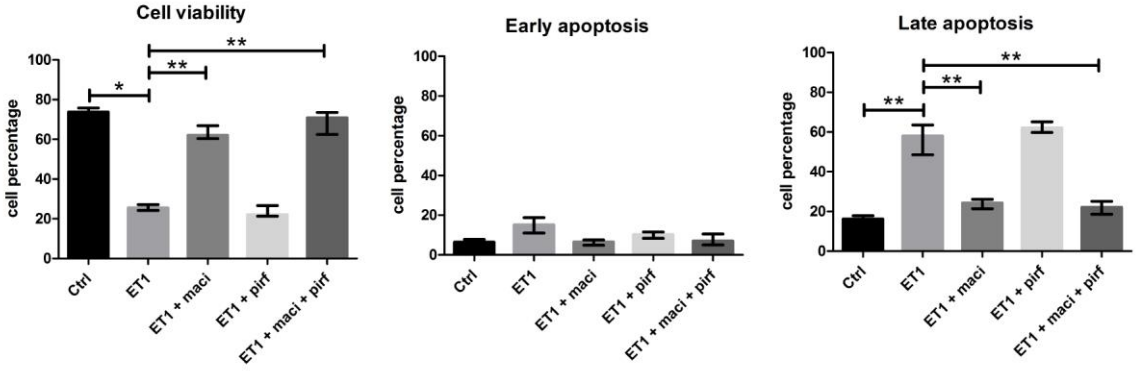

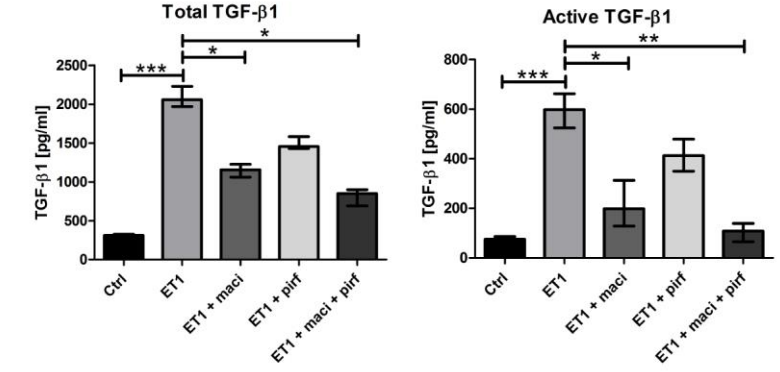

Supplemental Figure 6

A